Mineral Mountains West Fault System

June 30, 2019

MINERAL MOUNTAINS WEST FAULT SYSTEM

OUTLINE

1. SUMMARY

Geological, geophysical, and geochemical data, including new reprocessing of 3D seismic reflection data collected in 2017, have been reviewed in order to characterize the northern terminus of the Mineral Mountains West fault system.

This north-south system of relatively short fault strands is most clearly manifest on the surface as scarps on Pleistocene fan deposits, extending south of the Utah FORGE site. Within the Utah FORGE site, scarps are absent. Accordingly, the northern end of the Mineral Mountains West fault system terminates close to the southern boundary of the Utah FORGE site.

Comparison of east-west seismic reflection profiles within and south of the Utah FORGE site, support this interpretation for the subsurface as well. The seismic sections crossing the Utah FORGE site, which includes the well track of 58-32, shows no disruptions, offsets, or deformations in the granitic basement contact or overlying strata that might be taken as evidence of subvertical fault displacement to within a resolution of ~25 m. By contrast, an east-west legacy seismic profile 1 km south of the Utah FORGE boundary, shows tilted reflectors that are suggested to represent strata deformed by displacement along the Mineral Mountains West fault system.

Soil gas data indicative of structurally controlled hydrothermal fluid flow are confined to the east of the Opal Mound fault. By contrast, west of the Opal Mound fault including over the Mineral Mountains West fault system, the soil gas results show no hydrothermal activity. Accordingly, beneath the Utah FORGE site there is no evidence of advective fluid flow related to a connected network of subvertical faults and fractures crossing into the basement.

2. INTRODUCTION

The Utah FORGE site is an underground test facility for advancing EGS technologies. It is located 350 km south of Salt Lake City and 16 km north northeast of Milford, Utah. The site covers 5 km^2 (2 mi^2), and it is situated on a west sloping alluvial fan in northern Milford valley, roughly halfway between the crest of the Mineral Mountains to the east and the Beaver River to the west. The EGS reservoir, which is to be developed, is entirely hosted by fractured Tertiary granitoid rocks that form the basement unit to the northern Milford valley and that is also exposed throughout the core of the nearby Mineral Mountains.

The Utah FORGE site and nearby Roosevelt Hot Springs have been subject to a number of geoscientific investigations since the late 1970s, and a new phase of study commenced in 2015 as part of the process for site selection for the FORGE laboratory (Allis et al., 2016). In 2017, well 58-32 was drilled to 7536 ft depth to prove temperature and lithology, and to characterize fracture patterns and stress regime. The current state of knowledge is now underpinned by a wide range of geological, geophysical, and geochemical data derived from surface and well

measurements (Allis and Moore, 2019). One of the key conclusions is that no major active fault structures transect the FORGE site.

As part of an ongoing evaluation to provide an improved and state-of-the-art understanding of the geology, the evidence of fault structures in the immediate vicinity of the Utah FORGE site was reassessed. This work has been carried out to determine as accurately as possible the termination point of the northern segment of the Mineral Mountains West fault system and the magnitude of fault offset in the strands extending south of the project area. The results of this reassessment are described in this report, and they are based on geological, geophysical, and geochemical data collected through to present. Important to this effort is the reprocessing of the 3D seismic reflection survey (Miller, 2019, Appendix), which provides as clear of a picture as possible regarding vertical offsets in basin-fill stratigraphy and the underlying contact with the top of the basement granitoid.

3. GEOLOGICAL BACKGROUND

The north Milford valley is a broad sediment-filled basin that is bounded by the Star Range and Beaver Lake Mountains on the west and the Mineral Mountains on the east. Regional seismic reflection and gravity modeling illuminate the relatively simple geometry that defines the basin structure (Figs. 1-4). Figure 2 shows a seismic profile in which the top of the basement is clearly defined by two strong reflectors that dip in opposite directions towards each other. In the vicinity of the Utah FORGE site, gravity results indicate the east limb of this contact dips gently westward whereas the west limb dips steep eastward. In the north part of the valley (Figs. 3 and 4), this asymmetry may switch to the opposite side of the valley with the east limb dipping steeply westward and the west limb dipping gently westward (Fig. 3). From these regional surveys, the basement contact appears to be continuous, without any major structural breaks or offsets, including where it extends over the top of the EGS reservoir.

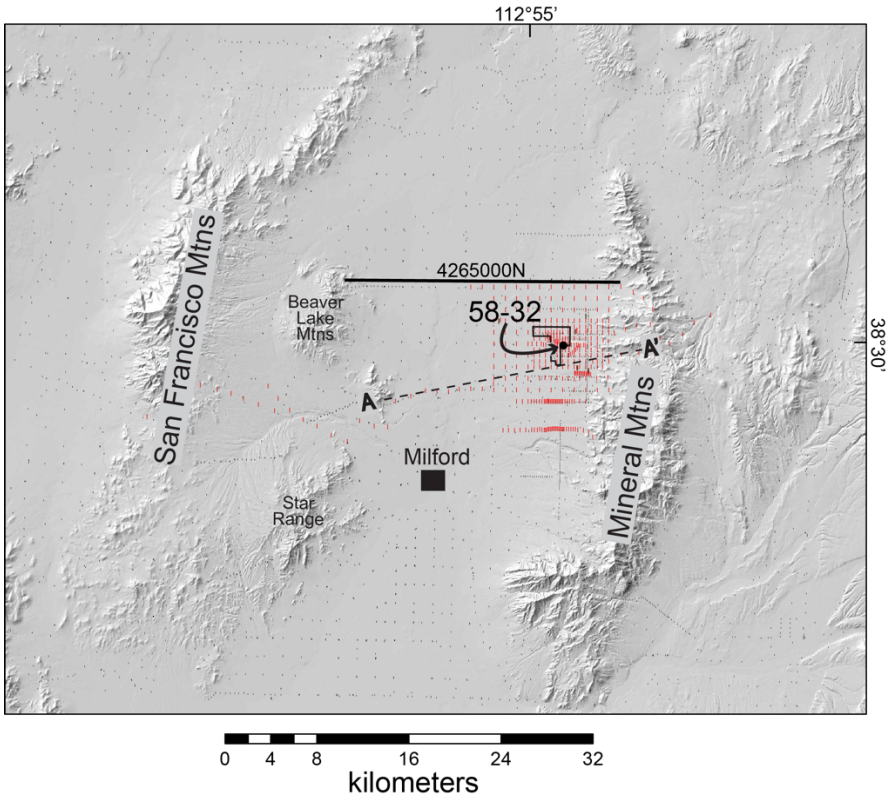

Figure 1. *Shaded relief map of the north Milford valley, showing the locations of the FORGE site, well 58-32, the seismic reflection line A-A', and the gravity model section line 4265000N. Data from 417 new gravity stations (red points) were acquired in Phase 2B, and the results were integrated with regional data (black points) to model the basin structure.*

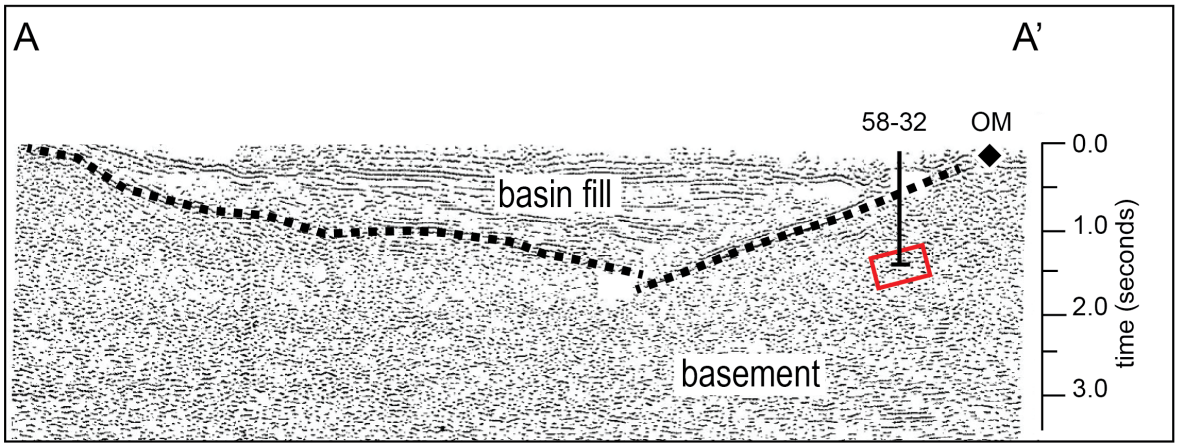

Figure 2. *Legacy seismic reflection profile, showing the geometry of the contact (bold dashed line) that separates basement rocks from the overlying basin fill (Smith and Bruhn, 1984; Smith et al. 1989). The vertical axis represents travel time rather than true depth, hence the vertical profile of 58-32 is approximated and projected on to the plane of the cross section. OM represents surface expression of the Opal Mound fault. Red box represents approximate position of the FORGE EGS reservoir.*

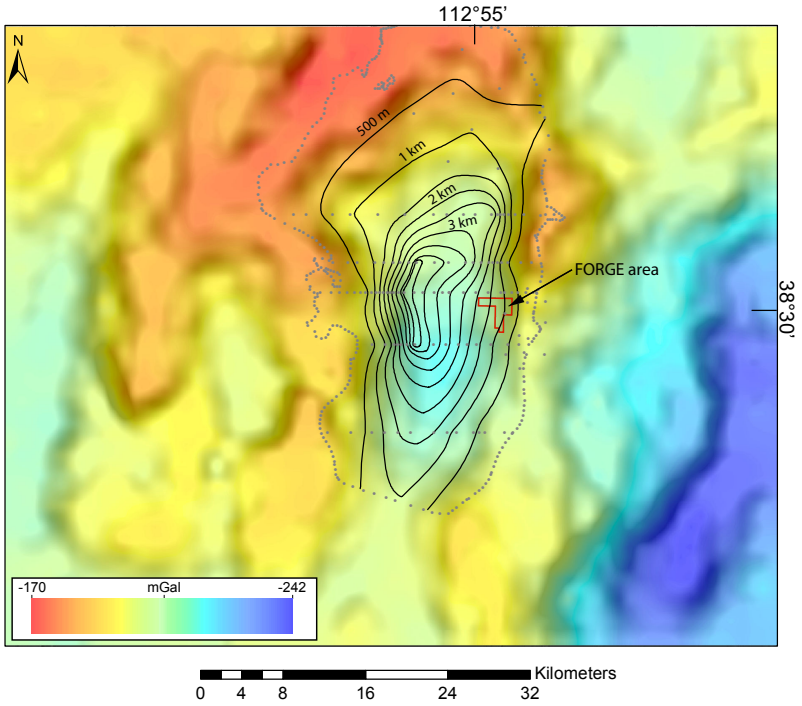

Figure 3. *Complete Bouguer Gravity Anomaly map, with shading generated from the horizontal gravity gradient, and the interpreted structure contours of the depth to basement (Hardwick et al., 2019). Contours are in 500 m increments and basement control points (gray dots) are from 2D gravity models, 1D MT models, and zero-depth picks on, or adjacent to, outcrop.*

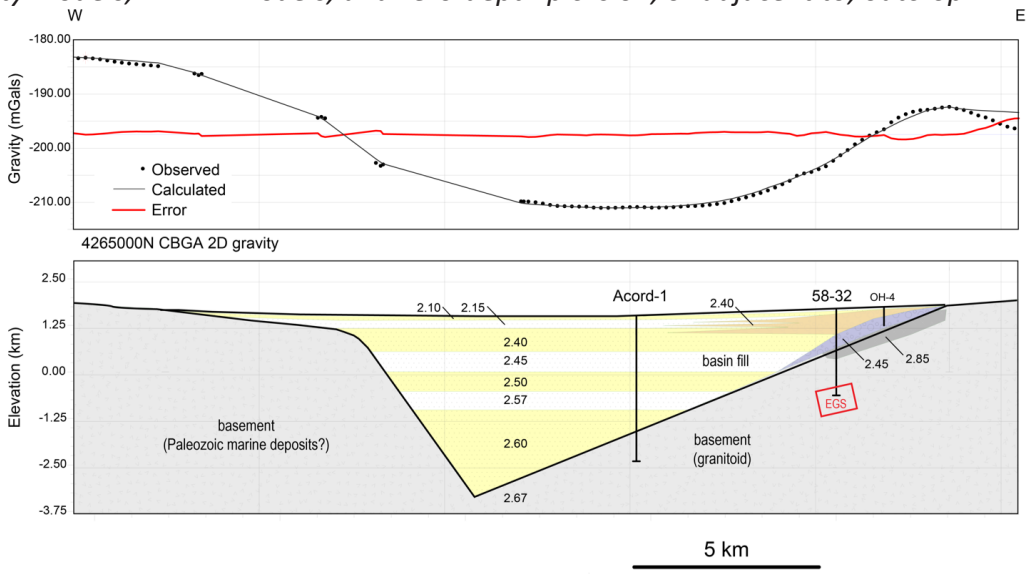

Figure 4. *Gravity model for section line UTM 4265000N, showing the basin structure and the densities of units that were used to calculate the complete Bouguer gravity anomaly (Webring, 1985; Hinze et al., 2005; after Hardwick et al., 2019). Density values were derived from existing well logs and lab measurements of surface samples and well cuttings/cores, including 58-32. Red box represents approximate position of the FORGE EGS reservoir.*

A. Stratigraphy

The regional stratigraphy comprises folded and imbricated Paleozoic-Mesozoic sedimentary strata, Tertiary igneous plutons, Tertiary-Recent volcanic deposits, and Tertiary-Recent basin fill sediments (e.g. Nielson et al., 1986; Coleman et al., 1997; Kirby, 2019). Near the Utah FORGE site, Paleozoic-Mesozoic strata are absent, and consequently the stratigraphy is divided into two broadly defined units, comprising crystalline plutonic rocks that form the basement and younger overlying bedded alluvium and volcanic deposits that fill the basin (Fig. 5).

The basement rocks are made of granitoids, which were emplaced between 26 and 8 Ma (Aleinikoff et al., 1987; Coleman, 1991; Coleman and Walker, 1992; Coleman et al., 2001). They represent products of magmatic processes, which most recently resulted in the eruption of young rhyolite centers (0.5-0.8 Ma) in the Mineral Mountains (Lipman et al., 1978). The granitoid plutons intruded tightly folded Precambrian gneiss (~1720 Ma), but only rafts of this older lithology are preserved, as seen in the western foothills of the Mineral Mountains and intersected in wells 9-1, 52-21, and 14-2 (Glenn and Hulen, 1979; Glenn et al., 1980; Nielson et al., 1986).

The basin fill consists of a layered sequence of sedimentary and volcanic deposits (>3000 m), which range from Tertiary to Recent in age. The strata from youngest to oldest consist of calcareous lacustrine siltstones and sandstones, volcaniclastic sandstones and gravels, tuffaceous deposits, and localized flows of andesitic lavas. On the surface, basin-fill deposits young from east to west, and the youngest ones, in the vicinity of well Acord 1, are composed of fine sediments and reworked alluvium that were deposited in Lake Bonneville (16-14.5 ka), whose shoreline is marked by wave cut escarpments and westward extending point bars. To the east including the area surrounding the FORGE site, late Pleistocene alluvial fans are mainly composed of pea-sized gruss, and scattered fragments of obsidian, derived from the Mineral Mountains. Across the Opal Mound fault, around the area of Roosevelt Hot Springs, the alluvium deposits are older, more than 0.8 Ma as constrained by dates on overlying flows of rhyolite (Lipman et al., 1978); the oldest alluvium likely dates back several million years, and it is restricted to a few isolated exposures (Kirby, 2019; Knudsen et al., 2019).

B. Faults

All of the faults in the vicinity of the Utah FORGE site are products of Basin and Range extension, mostly occurring in late Miocene time well after the main phase of plutonic intrusion (Coleman et al., 2001; Bartley, 2019). Four major faults and fault systems are known, based on field observations, seismic reflection, and correlation of drill logs (Kirby, 2019; Knudsen et al., 2019; Simmons et al., 2019).

The Opal Mound fault extends for ~5 km in a NNE direction, branching in the northernmost part. It has an inferred steep eastward dip (e.g. Nielson et al., 1986); however, the total displacement is difficult to measure, and it could be up to 15 m. The Opal Mound fault marks the western boundary of the Roosevelt Hot Springs hydrothermal system and importantly

forms a hydrological barrier to westward hydrothermal flow as revealed by pressure profiles from wells either side of the fault (Allis and Larsen, 2012; Allis et al., 2016). In the past, springs discharged from the southern and northern ends of the Opal Mound fault, but today surface activity is limited to steaming ground with acidic steam-heated water at its northern end. Before 1980, nearly neutral pH chloride water, resembling the reservoir composition, discharged at the surface (e.g. Capuano and Cole, 1982). Approximately 1600-1900 years ago, the discharge of nearly neutral pH thermal water was localized around the south end of the fault, depositing a thick sheet of silica sinter that marks the Opal Mound (Lynne et al., 2005).

The Negro Mag fault is an east-west striking structure that extends several kilometers eastward from intersection with the Opal Mound fault. This relatively short fault can be traced on the surface over a distance of ~1 km where it offsets an old alluvial fan deposit, creating an east-west ridge in the middle of Negro Mag wash. Judging from the orientations of numerous east-west trending joints and fractures in the Mineral Mountains, the fault is probably vertical, with an offset of <10 m downward on the north side (Kirby, 2019; Knudsen et al., 2019).

The Mineral Mountains West fault system, which is the subject of this report, represents a corridor of north-south trending fault scarps that are mappable on fan deposits south of the FORGE site. The system is up to 3 km wide, and it runs for at least 40 km, west of and parallel to the range front along the southern part of the Mineral Mountains. Individual strands are marked by scarps, generally having heights <5m, that form coherent traces up to 3 km long. Further information about the northern segment of this fault system is described below.

The most significant fault in the vicinity of the FORGE site is marked by the contact between overlying basin fill and the underlying crystalline basement rock (labeled “fault-unconformity-”, Fig. 5). It forms an inclined undulating ramp that dips 20-35° west and intersects the surface near the Opal Mound fault. This and related subparallel structures in the basement are believed to have accommodated large-scale down-dip displacement of >10 km (Bartley, 2019). The evidence that supports such interpretation includes seismic reflection data, regional outcrop patterns, the uniform eastward dip of stratified rocks in the Mineral Mountains, the uniform westward dip of late Miocene dikes in the Mineral Mountains, paleomagnetic data, and cooling patterns interpreted from thermochronology (Smith and Bruhn, 1984; Nielson et al., 1986; Smith et al., 1989; Coleman and Walker, 1992, 1994; Coleman et al., 2001). Furthermore, thin section of analysis of 58-32 drill cuttings shows clear evidence of intense shearing, brecciation, and cataclasis in the footwall directly beneath the basement contact (Jones et al., 2019). Most of the extension accommodated along this and related structures occurred during a short period of accelerated displacement in the late Miocene (10-8 Ma), which resulted in uplift, exhumation, and tilting (Nielson et al., 1986; Coleman and Walker, 1994; Coleman et al., 2001). What is now a shallow dipping fault surface probably initiated as a moderate to steeply dipping plane (Wernicke and Axen, 1988; Buck, 1988; Coleman and Walker, 1994; Bartley, 2019). Once the surface and related subparallel structures acquired shallow dips, the propensity for new fault slips greatly diminished because of cohesion. Erosion derived sediments probably started covering this surface shortly after movement ceased.

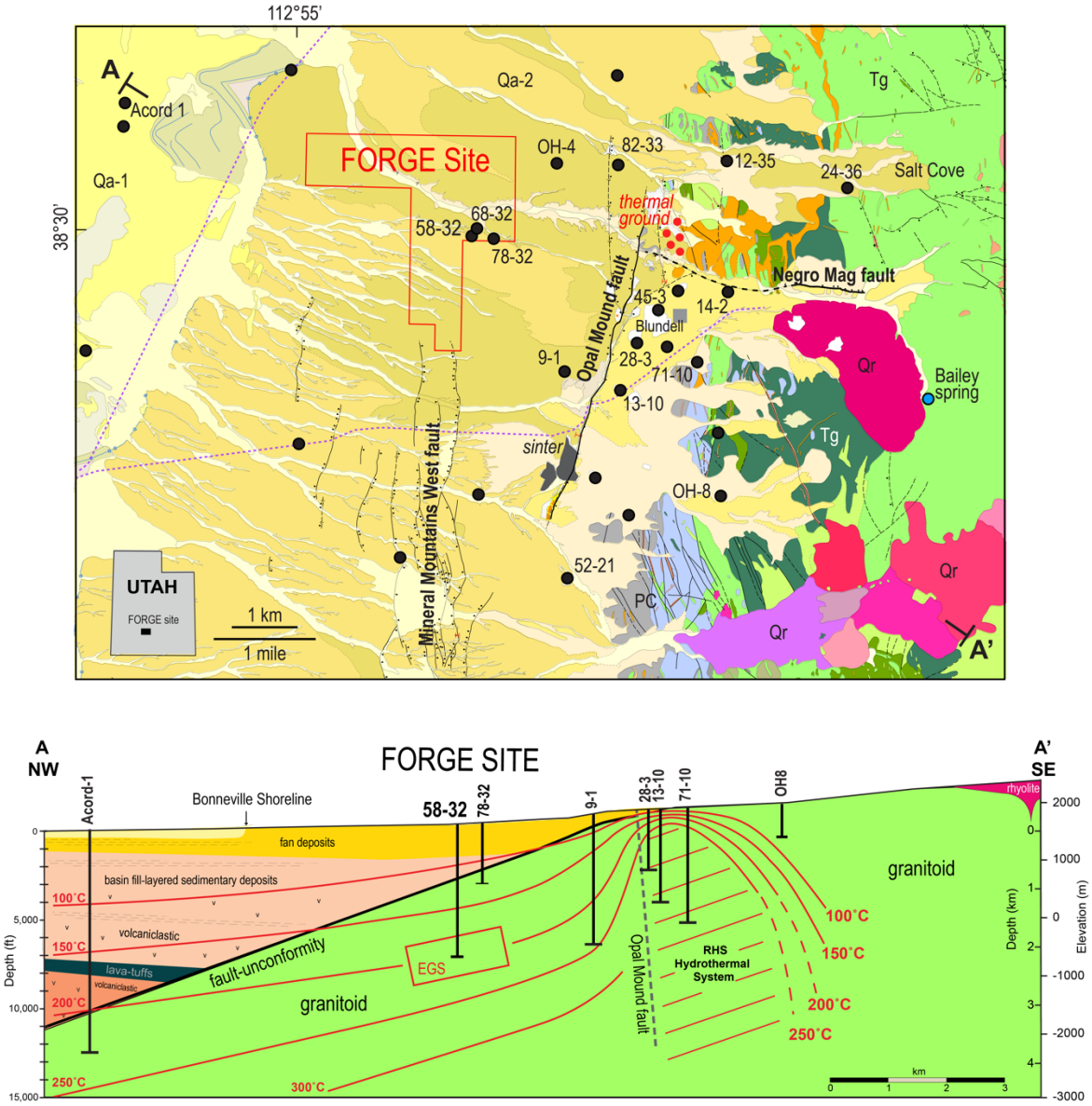

Figure 5. *Geological map and cross section for the FORGE Utah site (Simmons et al., 2019) based on the compilation of new field observations, well data, and previous work (Nielson et al., 1986; Kirby, 2019). The rhyolite flow (red) west of Bailey spring makes up Bailey ridge. Abbreviations: Qa-1=Lake Bonneville silts and sands; Qa-2=alluvial fan deposits; Qr=Quaternary rhyolite lava and pyroclastic deposits; Tg=Tertiary granitoid; PC=Precambrian gneiss; black filled circles=wells. In cross section, the red box represents approximate position of the FORGE EGS reservoir; RHS=Roosevelt Hot Springs.*

4. MINERAL MOUNTAINS WEST FAULT SYSTEM IN THE VICINITY OF THE FORGE SITE

Three independent field datasets have been acquired and analyzed to determine the northern terminus of the Mineral Mountains West Fault system in relation to the Utah FORGE site. They include: 1), geomorphic analysis of scarps on the alluvium fan surfaces, using LiDAR, field observations, and Infrared Stimulated Luminesce (IRSL) geochronology; 2), a 3D seismic reflection survey, the results of which have been reprocessed; and 3), CO_2 flux and He isotope soil gas analysis.

A. Surface Mapping and Geomorphic Analysis

Geomorphic analysis of faulting is based on field mapping and a high-resolution LiDAR 0.5-m bare-earth digital elevation model (DEM) of the Milford Valley and adjoining the Mineral Mountains acquired in the fall of 2016 (Fig. 6). Geologic mapping was done at 1:10,000 scale in conjunction with analysis of the LiDAR image from August to December of 2017. Black and white and color aerial photography of various ages and scales (1953 AMS, 1:63,300 scale; 1955 GS-VJI, 1:37,400 scale; 1979 CSR-F, 1:25,000 scale) were also reviewed. Many prominent lineaments and tonal changes on the photos—some of which that were mapped as faults by some previous mappers—are the result of extensive range-management and fire-suppression/mitigation efforts in the area that have spanned several decades. Some of the alluvium surfaces were also dated using Infrared Stimulated Luminescence (IRSL; Knudsen et al., 2019).

Slope maps, hill shade models from different sun angles, slope and aspect maps, and elevation contours were generated from the LiDAR DEM. To analyze fault scarp morphologies along strike, elevation profiles were generated in Global Mapper v.14. Using a slope map, topographic profiles were produced perpendicular to fault scarps with sufficient length to ensure complete capture of undeformed alluvial fan surfaces on the hanging wall and footwall of the faults (Fig. 7). To illustrate what is manifest in the field, a photograph of a segment of fault scarp is shown in Figure 8.

The northern segment of the Mineral Mountains West fault system extends for about 8 km, forming a structurally complex graben that ranges in width from ~700 – 1200 m with internal horst and graben blocks (Fig. 6). The fault system is defined by discontinuous, cuspate, short segment scarps up to 3 km long on late Pleistocene alluvial fans. Within the Utah FORGE site, there is no evidence of these scarps, and the northern terminus of the fault system coincides with the southern edge of the site (Fig. 6). The highest and most continuous scarps are west-dipping with ~1 to 8 m of offset and a normal sense of displacement. East-dipping scarps have an average height of 3.18 m and a slope of 5°, and west-dipping faults have an average height 3.16 m and slope of 7° (Fig. 7). The heights and slopes of both east-and-west-dipping scarps increase southward and, south of Corral Canyon, multiple strands of the fault zone converge into a single fault that has produced a scarp as high as about 12 m. The scarps are deeply dissected and display similar morphologies to the nearby Bonneville shoreline that formed about 16-14.5 ka, and this combined with the observation that parts of the fault zone are

covered by latest Pleistocene to Holocene alluvium indicate that the most recent movement on the fault zone is late Pleistocene (Knudsen et al., 2019). The maximum ages of fault slip on the Mineral Mountains West fault system range from 41 to 80 Ka based on two IRSL dates (Knudsen et al., 2019). The only other fault structure in alluvial fan deposits lies 2 kilometers north of the Utah FORGE site, and it comprises a short length (1.6 km) normal fault scarp, which trends north-northeast and dips west; all other fault structures north of the site are hosted in bedrock (Knudsen et al., 2019).

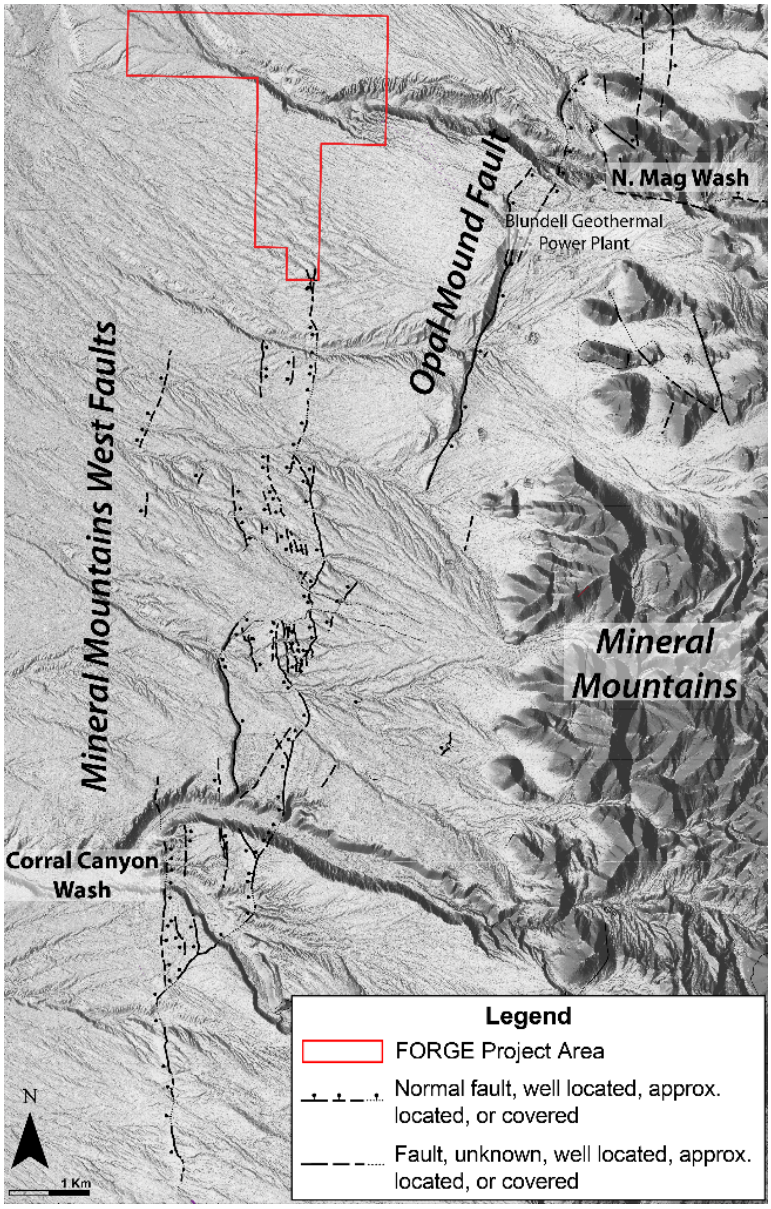

Figure 6. *Half-meter slope-shade LiDAR image showing the faults south and east of the Utah FORGE site. The northern extent of the Mineral Mountains West fault system forms a graben structure, with internal horsts and grabens which terminate near the southern Utah FORGE boundary.*

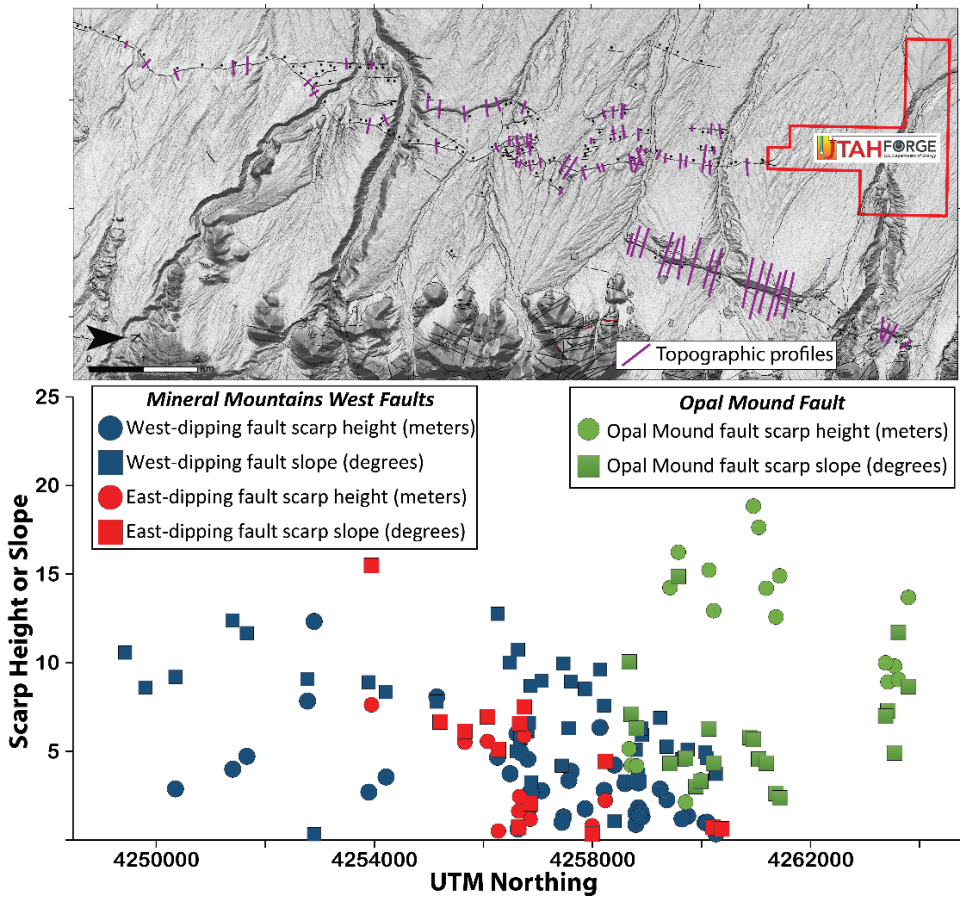

Figure 7. *Slope-shade image of the western Mineral Mountains showing location and extent of fault-scarp elevation profiles; note the compass azimuth is rotated 90°clockwise, with north heading right and south heading left. Graph shows fault scarp height and slope along strike traces of the Mineral Mountains West and the Opal Mound faults.*

Figure 8. *Low-morning sun angle view of a low MMW fault scarp (<5 m high) formed on late Pleistocene alluvial-fan deposits north of Ranch Canyon. The Mineral Mountains range front is nearly 2 miles distant from the scarp. View is to the southeast.*

B. 3D Seismic Reflection Survey

A 3D seismic reflection survey was acquired under subcontract to Paragon Geophysical Inc in November, 2017 (Fig. 9; Miller et al., 2019). Because the original delivered seismic processing results were considered incomplete, a reprocessing was undertaken by Land Seismic Noise Specialists (LSNS). The reprocessing includes two legacy seismic lines, 5 and 11, adjacent to the FORGE site (Fig. 9). Special attention was paid to the prestack removal of noise such as ground roll and any other noise identified by testing. In addition, depth imaging was performed. The complete report of this reprocessing and analysis is provided in the Appendix, which documents two problems that had to be overcome. The first involved creating a refraction statics solution to compensate for unusually large lateral variations in near surface velocity. The second involved severe random and coherent noise issues. LSNS used proprietary software to identify and filter out consistent and repeatable noise patterns in the shot and receiver domains of the data. This analysis revealed that the velocities of the basin fill sediments above the basement were directionally dependent, and thus warranting an anisotropic velocity model for depth migration.

A comparison of the 3D processing progression is shown for inline profile IL-93 (location in Fig. 9), which passes through well 58-32 (Figs. 10 and 11). In Figure 10, the top image shows the unmigrated time section, and the bottom image shows the prestack migrated time section. These time sections indicate that the basement contact reflector is laterally continuous, with no vertical offsets within the resolution of the seismic data. The absence of diffractions in the top unmigrated time section (Fig. 10) is another indication that no vertical offsets were detected. Figure 11 shows the prestack depth migration of IL-93, using the anisotropic migration. Again, the basement contact reflector is laterally continuous. Figure 12 shows the north-south prestack depth migration of XL-105 through well 58-32, in which the basement reflector is subdued with gentle undulation.

The resolution of vertical offsets across the basement contact is determined using the ¼ wavelength principle (Yilmaz, 2001), which states that the minimum detectable offset is approximately ¼ of the dominant frequency of the seismic wavelet. In the reflection survey, the dominant frequency of the data is 30 Hz (f) and the velocity immediately above the top of basement granitoid is 3000 m/s (v). Therefore, the wavelength, v/f, is 100 m. Accordingly, using the ¼ wavelength principle, offsets in the granite reflector of 25m or greater should be detectable. This principle is a function of the recording process and the earth properties; a primary achievement of the reprocessing done by LSNS was to extend the domain of this resolution due to superior noise removal and an improved velocity model.

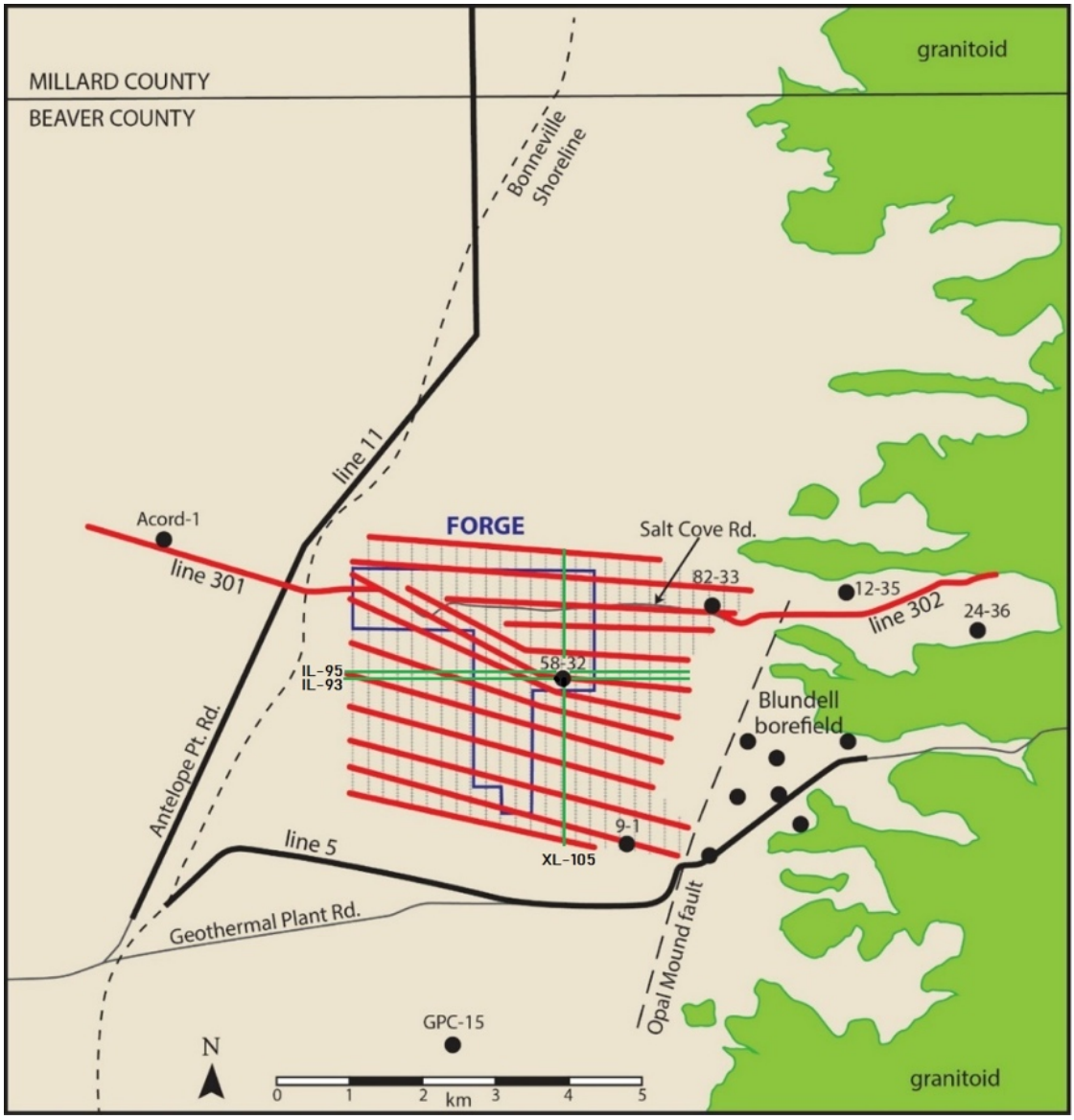

Figure 9. *Seismic survey profile locations (Miller et al., 2019; Miller report, Appendix). The 3D survey area comprises 13 red source lines (vibrator point locations 50 m apart), and 27 gray geophone lines geophone locations (oriented N-S, geophone interval 50 m). Red lines 301 and 302 are new 2D seismic lines; heavy black lines labeled 5 and 11 are legacy 2D lines licensed from Seismic Exchange, Inc. Green lines are 3D inlines (IL) and crosslines (XL) that intersect at well 58-32.*

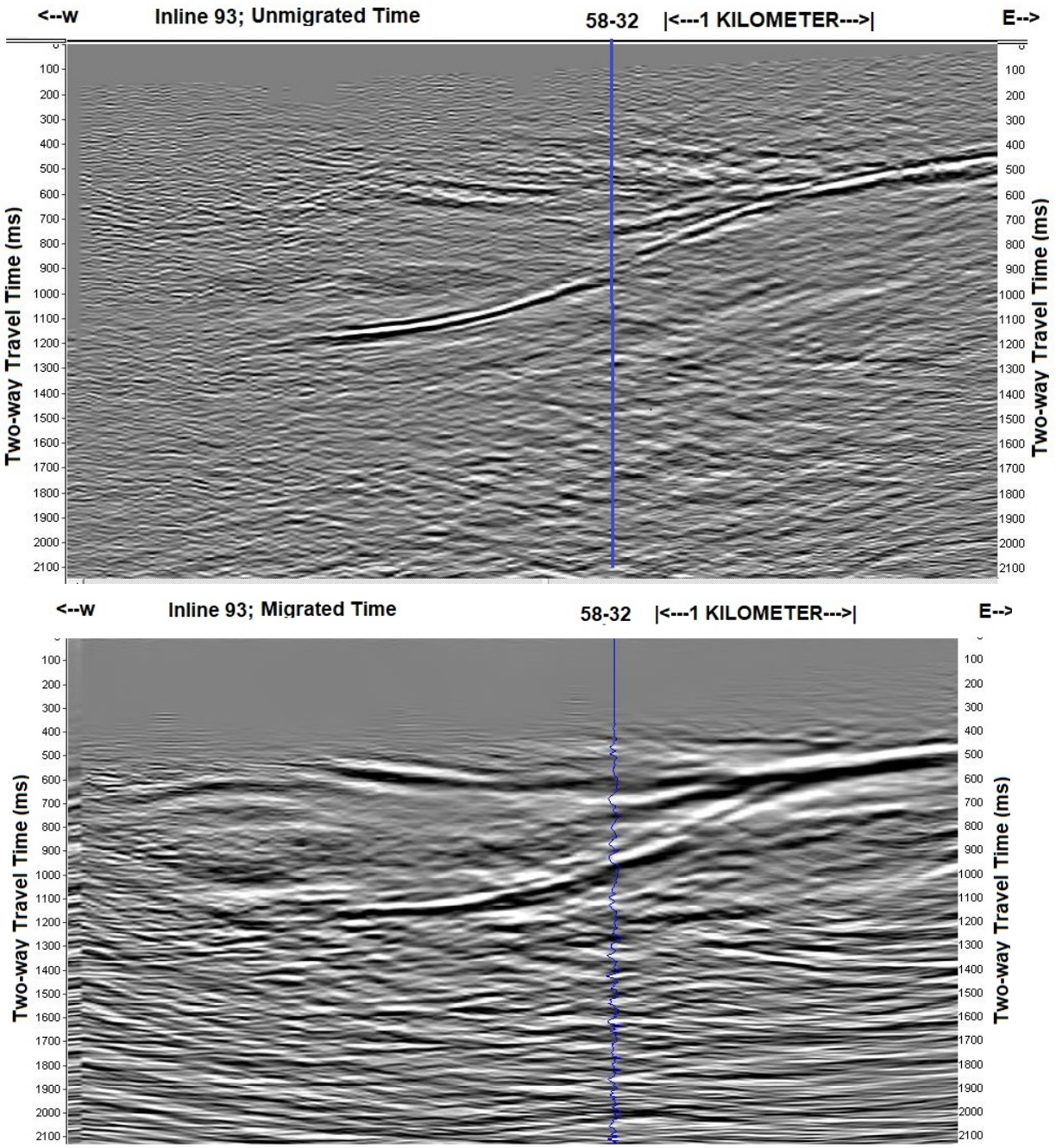

Figure 10. *Top: Unmigrated Time processing for IL-93. Bottom: Migrated time version of top, showing a horizontally continuous reflection from the top of basement with no detectable vertical offsets. The location of well 58-32 is shown in blue.*

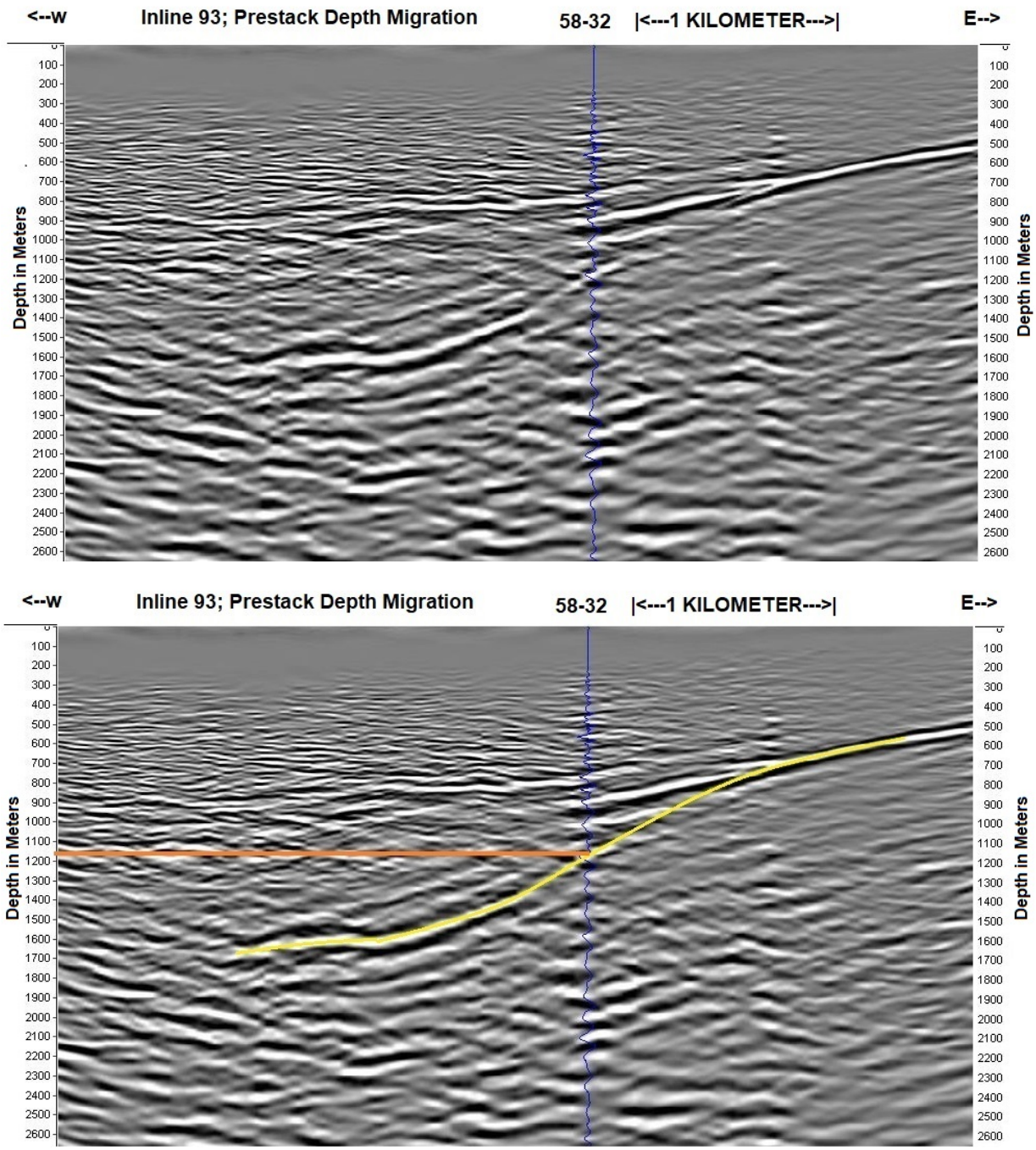

Figure 11. *Top) Uninterpreted estimated anisotropic prestack depth migration; bottom) Interpreted version of the top. Yellow line indicates interpretation of the top of basement reflector. The horizontal orange line indicates the basement intersection in 58-32, which is shown in blue. Depth is referenced to a datum at 1800 m asl.*

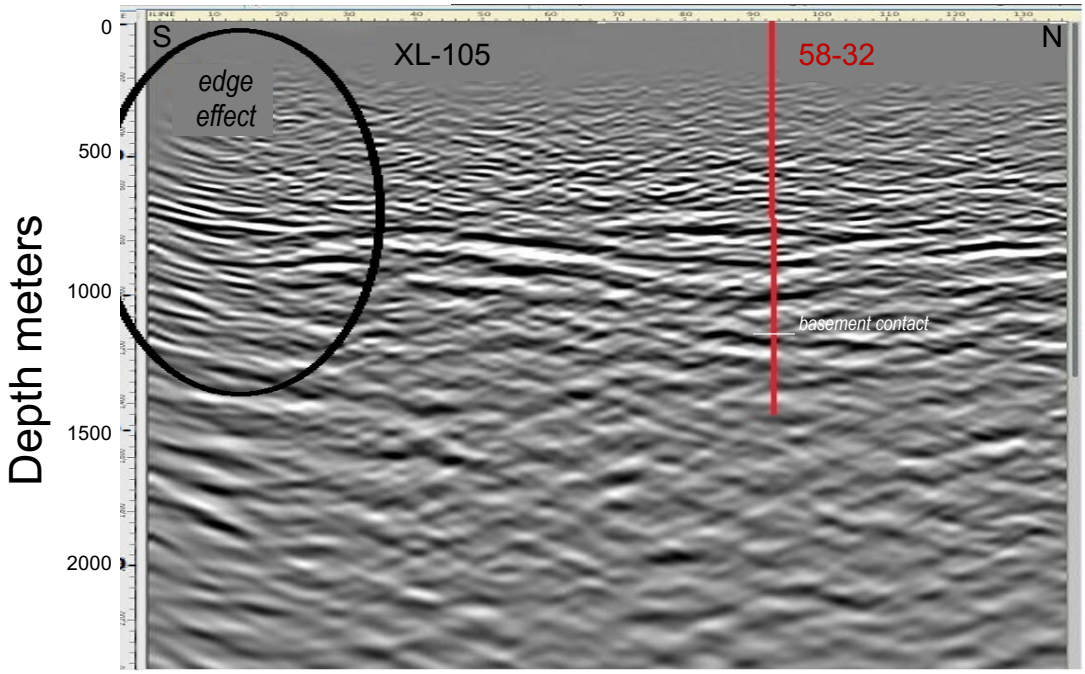

Figure 12. *North-south prestack depth migration through 58-32. Depth is referenced to a datum at 1800 m asl.*

C. CO_2 Flux and Helium Isotopes of Soil Gas

As a check on cryptic fluid flow through fault-controlled structures, soil gas surveys were performed in June 2017 and January 2018 (Rahilly et al., 2019). The CO_2 flux across the Utah FORGE site and the Mineral Mountains West fault system was determined using a PP Systems Environmental Gas Monitor 5 (Figs. 13 and 14). To overcome sensitivities related to weather conditions and/or frozen ground, the results were normalized against the biogenic background flux to give consistent values (e.g., Lewicki et al., 2005). Values above the background flux are classified as anomalous and related to geothermal fluid flow (e.g., Chiodini et al., 1998).

A separate helium isotope soil gas survey was performed in November 2017 using diffusion samplers. These samplers were placed into the bottoms of piezometers (2-3' long and 1" diameter stainless steel tubes), which were inserted into holes dug with an auger tool and backfilled with compacted soil. The piezometer was sealed with a threaded galvanized steel cap. After 9-10 days, the samplers were retrieved and crimped within 1 minute of being exposed to atmosphere to seal the copper capsule containing the gas sample. When retrieved, all the piezometers were dry. All of the samples were analyzed for helium and neon isotopes at the University of Utah Dissolved and Noble Gas Lab on a magnetic sector field mass spectrometer, and the precision for these analyses is 1.5 and 2.0%, respectively. Measured $^3He/^4He$ ratios are normalized using the atmospheric value ($Ra=1.386x10^{-6}$, Ozima and Podosek, 1983), and only four soil gas samples from east of the Opal Mound fault were corrected for atmospheric contamination (Rahilly et al., 2019).

A summary of results is shown in Figure 15, which clearly shows the absence of anomalous CO_2 fluxes anywhere west of the Opal Mound fault, including the Utah FORGE site and across strands of the Mineral Mountains West fault system. For comparison east of the Opal Mound fault, soil gases show high CO_2 fluxes and mantle helium isotope signatures coinciding with hydrothermal fluid flow.

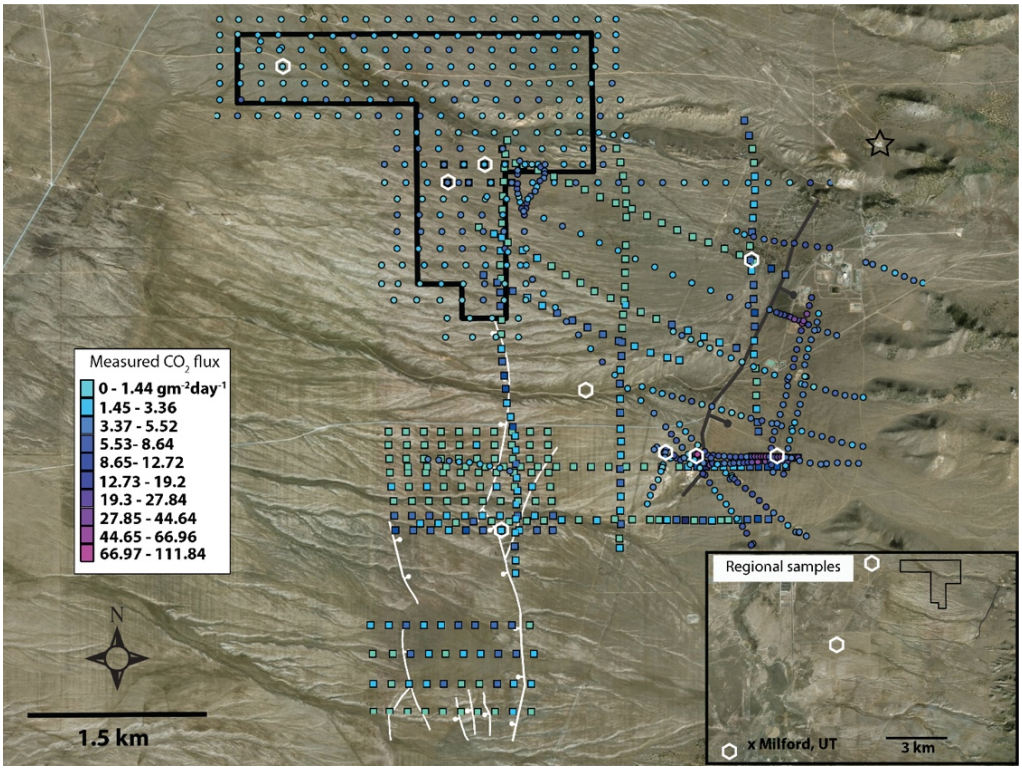

Figure 13. *Sample sites for CO_2 flux measurements from June (circles) and January (squares) across the FORGE project (black polygon), Opal Mound fault (dark gray line), and Mineral Mountains West faults (white lines). White hexagons are the locations of gas samples collected for $\delta^{13}C$ isotope composition analysis (Rahilly et al., 2019). The locations of regional gas samples are in inset. The black star represents Roosevelt Hot Springs.*

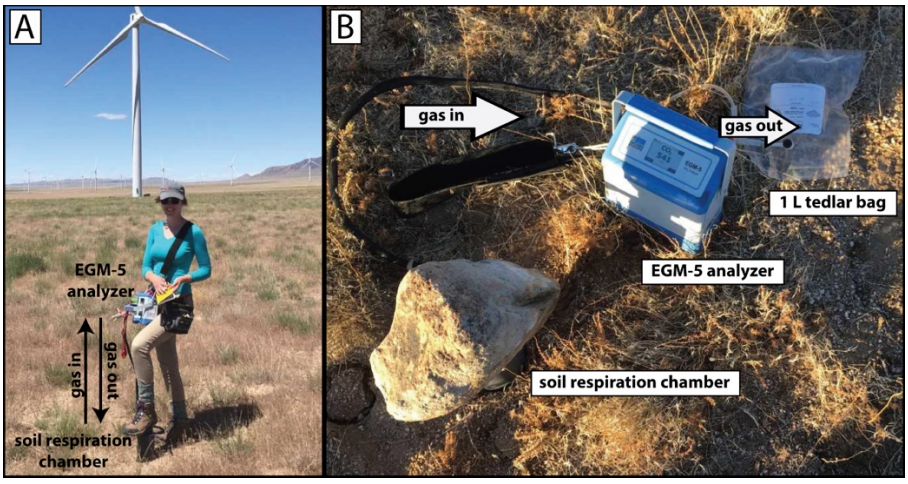

Figure 14*. A) Field deployment of EGM 5 instrument with soil respiration chamber. B) EGM 5 with Tedlar bag connected to gas-out port for collection of soil gas samples.*

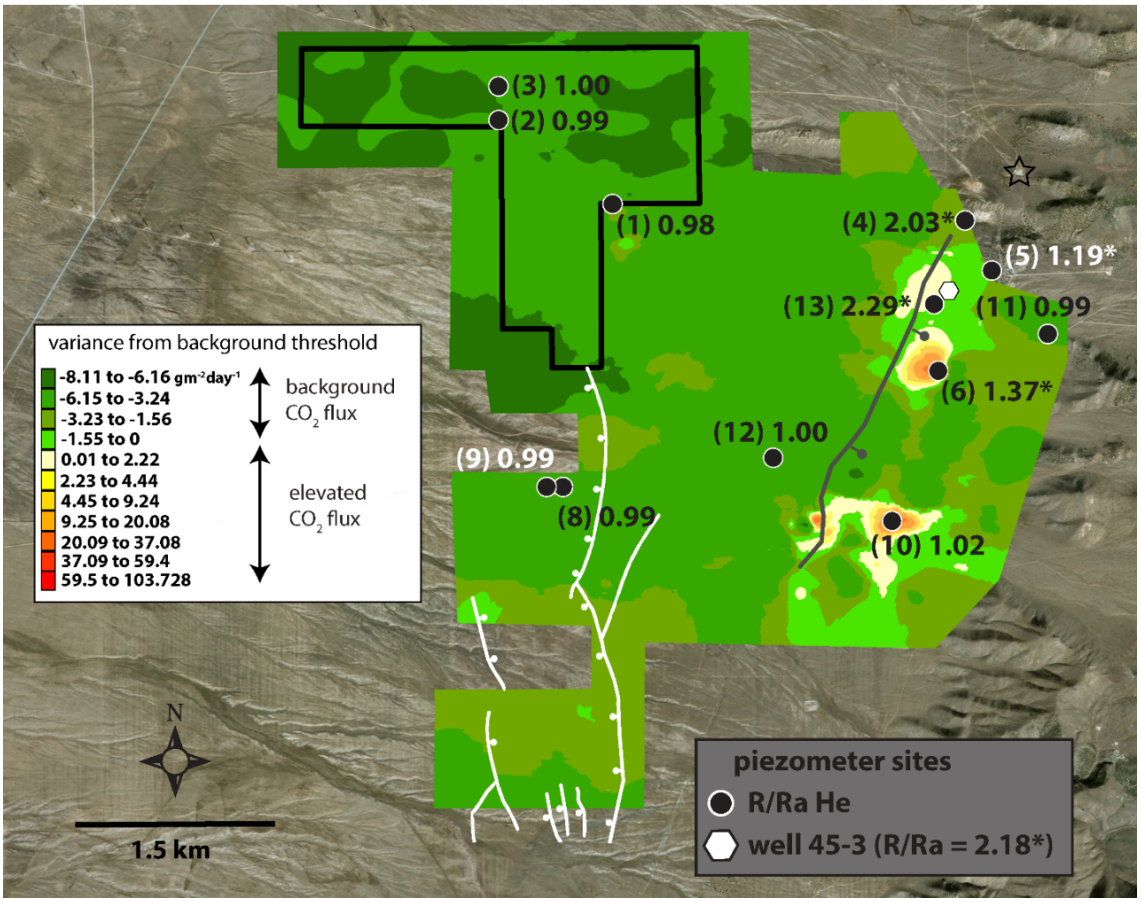

Figure 15. *Contoured soil CO_2 fluxes and helium isotope (R/Ra) soil gas measurements (asterisks indicate values that have been corrected for air contamination). FORGE site is the black polygon, Opal Mound fault is the dark gray line, and scarps of the Mineral Mountains West fault are the white lines. The biogenic background threshold was determined using the statistical population distribution method (Sinclair, 1974)*

5. DISCUSSION

The Mineral Mountain West fault system is recognized solely on the basis of surface mapping, and it is distinct in character from the Opal Mound and Negro Mag Wash faults (Knudsen et al., 2019). It comprises a complex system of discontinuous structures that form relatively short strands (<3 km), marked by scarps with relatively small offsets (<5 m). The geometry and orientation indicate that it dates back to at least 40-80 ka based on IRSL analyses, with no new movement since late Pleistocene. Importantly and as far as can be determined, the Mineral Mountains West fault system terminates near the southern boundary of the Utah FORGE site, and there is no evidence of these scarps north of this boundary (Figs. 6 and 7).

Seismic reflection data confirm the absence of subvertical structures beneath the Utah FORGE site. The reprocessed images show the continuous nature of horizontal reflectors that mark stratigraphic and bedding contacts in the basin fill stratigraphy (Figs. 10, 11. and 12). The strongest reflector marks the top of basement contact and it too is continuous (Figs. 10 and 11). Compared to LiDAR and surface mapping, the vertical resolution of stepped offsets in the seismic reflection data is much coarser and limited to about 25 m (Miller, 2019; Appendix). However, if the sediments immediately contacting the basement interface were laid down nearly syn-tectonically with interface development, then at most 25m of offset would be constrained to have occurred since 10-8 Ma.

In addition, in this regard it is useful to compare the sections in Figures 10 and 11 with those in Figure 16, which represent the 2D legacy seismic reflection profiling along line 5 (Fig. 9). The legacy and 2019 processing show the correlation between position of tilted reflectors in the basin fill strata and the location of a strand the Mineral Mountains West fault system (Fig. 16). Accepting that these images represent moderately dipping stratigraphic contacts, then subsurface seismic reflection evidence of the Mineral Mountains West fault system appears to exist in the form of deformation rather than stepped offsets. The seismic reflection data are thus entirely consistent with the observations of fault scarps on the surface, confirming the absence of detectable subvertical fault traces beneath the Utah FORGE site.

The soil gas data provide no indication that the Mineral Mountains West fault system extends into basement rocks where they might tap fluids or gases. Instead, these data indicate the absence of any structurally controlled hydrothermal fluid flow west of the Opal Mound fault, in contrast to soil gas results measured east of the Opal Mound fault (Fig. 15).

The overall impression gained from this analysis is that the Mineral Mountains Fault system is a relatively small-scale geologic structure in the context of Basin and Range faults. Total offset is minimal, perhaps as much as 15 m, but this is where the fault system is much better developed 6 km south of the Utah FORGE site (Fig. 7). Judging from Figure 16, the fault system seems to be entirely hosted within the basin fill strata, soling into the top of basement contact. If this is correct, then it is entirely possible that the faults represent minor listric structures that accommodate modern day tectonic stresses including gravity slumping in a relatively subdued extensional regime.

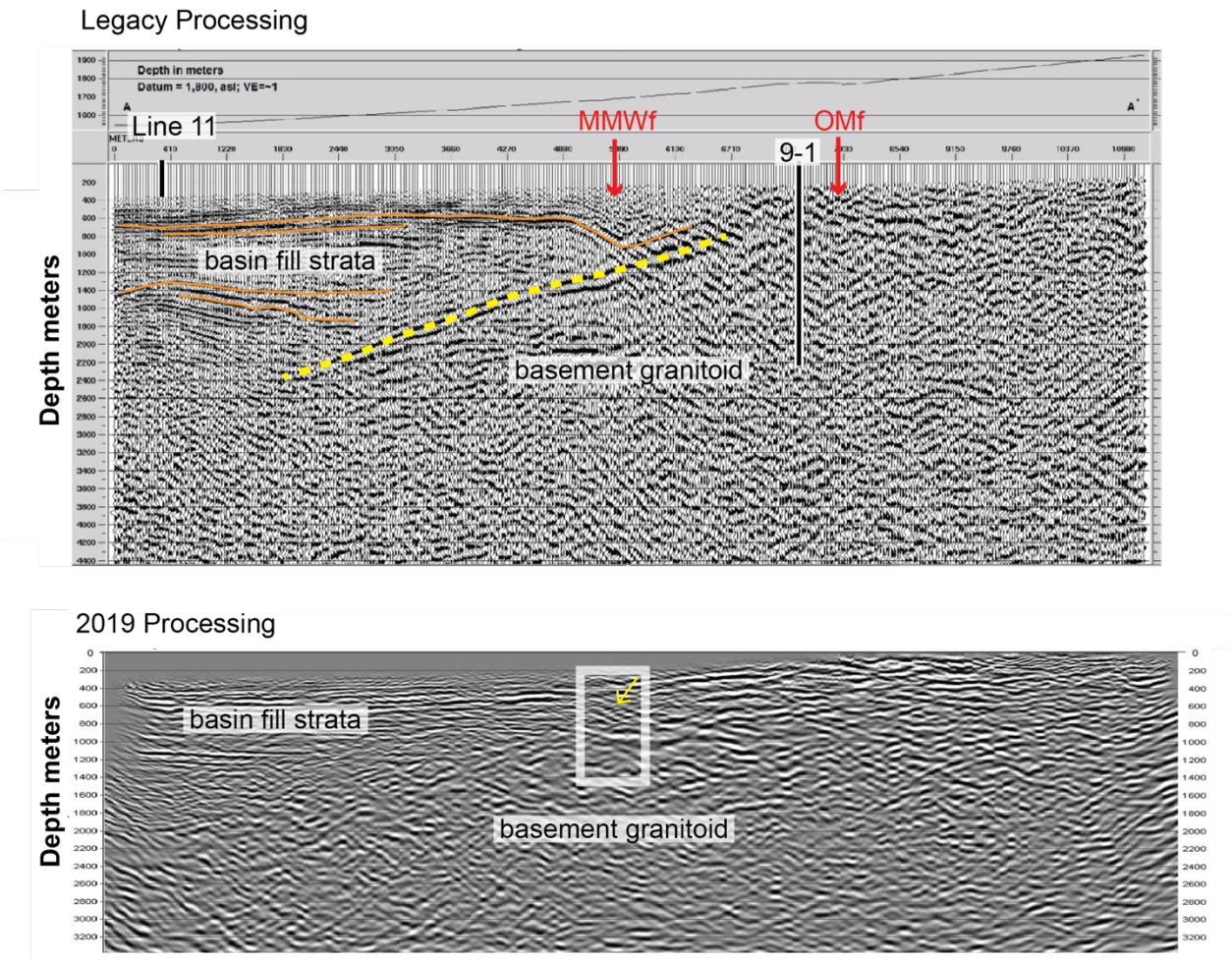

Figure 16. *Depth migrated 2D seismic profiles line 5 representing legacy and 2019 processing. Depth is referenced to a datum at 1800 m asl. There is no vertical exaggeration. Intersections with line 11, and traces of the Mineral Mountains West fault system and Opal Mound fault are indicated. In the 2019 processing, the yellow arrow and surrounding white box indicate zone of tilted reflectors in the basin fill strata that are clearly visible in the legacy processing. Abbreviations: MMWf=Mineral Mountains West fault system; OMf=Opal Mound fault.*

6. CONCLUSIONS

Evaluation of all the geoscientific data, including new reprocessing of 3D seismic reflection data collected in 2017, has been reviewed to characterize the northern terminus of the Mineral Mountains West fault system. This north-south system of relatively short fault strands is mapped in highest resolution on the surface represented by scarps on Pleistocene fan deposits. Within the Utah FORGE site, scarps are absent. Accordingly, the Mineral Mountains West fault system terminates near the southern edge of the Utah FORGE site.

Comparison of east-west seismic reflection profiles within and south of the Utah FORGE site, support this interpretation. The section crossing the Utah FORGE site, which includes the well track of 58-32, shows no disruptions, offsets, or deformations in the basement contact or overlying strata that might be taken as evidence of subvertical fault displacement. By contrast, the east-west profile 1 km south of the Utah FORGE boundary, shows titled reflectors that may represent strata deformed by displacement along the Mineral Mountains West fault system.

Soil gas data indicative of structurally controlled hydrothermal fluid flow are confined to the east of the Opal Mound fault. By contrast, west of the Opal Mound fault including over the Mineral Mountains West fault system, the soil gas results show no hydrothermal activity. Accordingly, beneath the Utah FORGE site there is no evidence of advective fluid flow related to a connected network of subvertical faults and fractures crossing into the basement.

7. CONTRIBUTING AUTHORS

Stuart Simmons, Phil Wannamaker, John Miller, Tyler Knudsen, Kristen Rahilly, Emily Kleber, Stefan Kirby, Christian Hardwick, and Clay Jones

8. REFERENCES

Allis R. G. and Larsen, G. 2012. Roosevelt Hot Springs Geothermal field, Utah – reservoir response after more than 25 years of power production. Proceedings, 37th Workshop on Geothermal Reservoir Engineering, Stanford University, Stanford, CA, 8 p.

Allis, R.G., Gwynn, M., Hardwick, C., Kirby, S., Moore, J., and Chapman, D. 2015. Re-evaluation of the pre-development thermal regime of Roosevelt Hot Springs geothermal system, Utah. Proceedings, 40th Workshop on Geothermal Reservoir Engineering, Stanford University, Stanford, CA, 12 p.

Allis, R.G., Moore, J.N., Davatzes, N., Gwynn, M., Hardwick, C., Kirby, S., Pankow, K., Potter, S., and Simmons, S.F., 2016, EGS Concept Testing and Development at the Milford, Utah FORGE

Site. Proceedings, 41st Workshop on Geothermal Reservoir Engineering, Stanford University, Stanford, CA, p. 886-898.

Allis, R., and Moore, J.N, 2019, Geothermal Characteristics of the Roosevelt Hot Springs System and Adjacent FORGE EGS Site, Milford, Utah. Miscellaneous Publication 169-C Utah Geological Survey, in press.

Aleinikoff, J.N., Nielson, D.L., Hedge, C.E., and Evans, S.H., 1987, Geochronology of Precambrian and Tertiary rocks in the Mineral Mountains, south-central Utah. US Geological Survey Bulletin, 1622, p. 1-12.

Bartley, J.M., 2019, Joint patterns in the Mineral Mountains intrusive complex and their roles in subsequent deformation and magmatism. Utah Geological Survey Miscellaneous Publication 169-C, 13 p., 1 appendix, https://doi.org/10.34191/MP-169-C. in press.

Buck, R.W., 1988, Flexural rotation of normal faults: Tectonics, v.7, p. 959-973.

Capuano, R. M., and Cole, D. R., 1982 Fluid-mineral equilibria in a hydrothermal system. Geochimica Cosmochimica Acta, 46, p. 1353-1364. 71

Chiodini, G., Cioni, R., Guidi, M., Raco, B., and Marini, L., 1998, Soil CO_2 flux measurements in volcanic and geothermal areas: Applied Geochemistry, v. 13, no. 5, p. 543–552.

Coleman, D.S., 1991, Geology of the Mineral Mountains batholith, Utah: Lawrence, University of Kansas, unpublished Ph.D. thesis, 219 p.

Coleman, D.S., and Walker, J.D., 1992, Evidence for the generation of juvenile granitic crust during continental extension, Mineral Mountains batholith, Utah. Journal of Geophysical Research, v. 97, p. 11011-11024.

Coleman, D.S., and Walker, J.D., 1994, Modes of tilting during extensional core complex development: Science, v. 263, p. 215-218.

Coleman, D.S., Walker, J.D., Bartley, J.M., and Hodges, K.V., 2001, Thermochronologic evidence for footwall deformation during extensional core complex development, Mineral Mountains, Utah *in* Erskine, M.C., Faulds, J.E., Bartley, J.M., and Rowley, P.D., editors, The geologic transition, High Plateaus to Great Basin—a symposium and field guide (The Mackin Volume): Utah Geological Association and Pacific Section of the American Association of Petroleum Geologists, Utah Geological Association Publication 30, p. 155–168.

Glenn, W.E., and Hulen, J. B., 1979, Interpretation of well log data from four drill holes at Roosevelt Hot Springs KGRA. DOE Earth Science Laboratory Report, University of Utah, pp. 74.

Glenn, W.E., Hulen, J. B., and Nielson, D.L., 1980, A comprehensive study of LASL well C/T-2 Roosevelt Hot Springs KGRA, Utah, and applications to geothermal well logging. Los Alamos Scientific Laboratory Report, LA-8686-MS, pp 175.

Hardwick, C., Hurlbut, W., and Gwynn, M., 2019, Geophysical surveys of the Milford, Utah, FORGE site—gravity and TEM. Utah Geological Survey Miscellaneous Publication 169-F, 15 p., https://doi.org/10.34191/MP-169-F.

Hinze, W. J., Aiken, C., Brozena, J., Coakley, B., Dater, D., Flanagan, G., Forsberg, R., Hildenbrand, T., Keller, G. R., Kellogg, J., Kucks, R., Li, X., Mainville, A., Morin, R., Pilkington, M., Plouff, D., Ravat, D., Roman, D., Urrutia-Fucugauchi, J., Veronneau, M., Webring, M., and Winester, D., 2005. New standards for reducing gravity data: The North American gravity database. Geophysics, Vol. 70, No. 4, p.J25-J32.

Jones, C.G., Moore, J.N., and Simmons, S., 2019, Petrography of the Utah FORGE site and environs, Beaver County, Utah, *in* Allis, R., and Moore, J.N., editors, Geothermal characteristics of the Roosevelt Hot Springs system and adjacent FORGE EGS site, Milford, Utah: Utah Geological Survey Miscellaneous Publication 169-K, 23 p., 2 appendices, https://doi.org/10.34191/MP-169-K.

Kirby, S.M., 2019, Revised mapping of bedrock geology adjoining the Utah FORGE site. Utah Geological Survey Miscellaneous Publication 169-A, 6 p., 2 plates, scale 1:24,000, https://doi.org/10.34191/MP-169-A.

Knudsen, T., Kleber, E., Hiscock, A., and Kirby, S.M., 2019, Quaternary geology of the Utah FORGE site and vicinity, Millard and Beaver Counties, Utah. Utah Geological Survey Miscellaneous Publication 169-B, 21 p., 2 appendices, https://doi.org/10.34191/MP-169-B.

Lewicki, J.L., Bergfeld, D., Cardellini, C., Chiodini, G., Granieri, D., Varley, N., and Werner, C., 2005, Comparative soil CO_2 flux measurements and geostatistical estimation methods on Masaya volcano, Nicaragua. Bulletin of Volcanology, v. 68, no. 1, p. 76–90.

Lipman, P.W., Rowley, P.D., Mehnert, H.H., Evans S.H., Jr., Nash, W.P., and Brown F.H., 1978, Pleistocene rhyolite of the Mineral Mountains, Utah—geothermal and archeological significance: Journal Research U.S. Geological Survey, v. 6, p. 133–147.

Lipman, P.W., Rowley, P.D., Mehnert, H.H., Evans S.H., Jr., Nash, W.P., and Brown F.H., 1978, Pleistocene rhyolite of the Mineral Mountains, Utah—geothermal and archeological significance: Journal Research U.S. Geological Survey, v. 6, p. 133–147.

Lynne, B.Y., Campbell, K.A., Moore, J.N., and Browne, P.R.L., 2005, Diagenesis of 1900 year-old siliceous sinter (opal-A to quartz) at Opal Mound, Roosevelt Hot Springs, Utah. Sedimentary Geology, 179, 249-278.

Miller, J., Allis, R., and Hardwick, C., 2019, Interpretation of seismic reflection surveys near the FORGE enhanced geothermal systems site, Utah. Utah Geological Survey Miscellaneous Publication 169-H, 13 p., https://doi.org/10.34191/MP-169-H.

Nielson D. L., Evans, S.H., Jr., Sibbett, D.S., 1986, Magmatic, structural, and hydrothermal evolution of the Mineral Mountains intrusive complex, Utah: Geological Society of America Bulletin, v. 97, no. 6, p. 765-777.

Ozima, M. and Podosek, F.A., 1983, Noble gas geochemistry: Cambridge University Press, 367 p.

Rahilly, K., Simmons, S., and Fischer, T.P., 2019, Carbon dioxide flux and carbon and helium isotopic composition of soil gases across the FORGE site and Opal Mound fault, Utah, *in* Allis, R., and Moore, J.N., editors, Geothermal characteristics of the Roosevelt Hot Springs system and adjacent FORGE EGS site, Milford, Utah: Utah Geological Survey Miscellaneous Publication 169-I, 16 p., 1 appendix, https://doi.org/10.34191/MP-169-I.

Simmons, S.F., Kirby, S., Bartley, J., Allis, R., Kleber, E., Knudsen, T., Milller, J., Hardwick, C., Rahilly, K., Fischer, T., Jones, C., and Moore, J.N., 2019, Update on the geoscientific understanding of the Utah FORGE site. Proceedings, 44th Workshop on Geothermal Reservoir Engineering, Stanford University, Stanford, CA, 10 p.

Sinclair, A. J., 1974, Selection of threshold values in geochemical data using probability graphs: Journal of Geochemical Exploration, v. 3, no. 2, p. 129–149.

Smith, R.B., and Bruhn, R. L., 1984, Intraplate extensional tectonics of the eastern Basin-Range: Inferences of structural style from seismic reflection data, regional tectonics, and thermal-mechanical models of brittle-ductile deformation: Journal of Geophysical Research, v. 89, B7, p. 5733-5762.

Smith, R.B., Nagy, W.C, Julander, K.A., Viveiros, J.J., Barker, C.A., and Gants, D.G., 1989, Geophysical and tectonic framework of the eastern Basin and Range-Colorado Plateau-Rocky Mountain transition. Geological Society of America Memoir 172, p. 205-233.
Wallace, R. E., 1951. Geometry of shearing stress and relation to faulting. Journal of Geology, 59, 118-130.

Webring, M.W., 1985. SAKI--A Fortran program for generalized linear inversion of gravity and magnetic profiles: U.S. Geological Survey Open-File Report 85-122, 104 p.

Wernicke, B.P., and Axen, G.J., 1988, On the role of isostasy in the evolution of normal fault systems: Geology, v. 16, p. 848-851.

Yilmaz, O., 2001, Seismic Data Analysis: Processing, Inversion, and Interpretation of Seismic Data. Society of Exploration Geophysics, 2065 p., http://dx.doi.org/10.1190/1.9781560801580.

APPENDIX

Miller, J.J., 2019, 2018-2019 reprocessing of the 2D and 3D multichannel seismic surveys at the FORGE Utah EGS Laboratory. Internal Report, 34 pp.

2018-2019 reprocessing of the 2D and 3D multichannel seismic surveys at the FORGE Utah EGS Laboratory

By John J. Miller[1]

[1]Consulting Geophysicist, Golden, CO 80401

Introduction

In November 2017, a new ~7 mi^2 (~17 km^2) three dimensional (3D) multichannel seismic reflection survey and two 2.4 mile (4 km) long two dimensional (2D) multichannel seismic lines were collected over, and extending east and west from, the Utah FORGE site. In addition, in September and October 2017, two previously existing seismic lines (legacy 2D data) adjacent to the FORGE site, ~7 miles (11 km) and ~8.5 miles (14 km) long, were licensed from Seismic Exchange, Inc. (SEI) with limited publication rights. The locations of these data are given in Figure 1.

Utah FORGE personnel performed data enhancement and depth conversion on the SEI data in late 2017. The new 2D and 3D data were collected by Paragon Geophysical, of Wichita, Kansas, who subcontracted with Star Geophysics, Inc., of Oklahoma City, Oklahoma, to process these newly-collected data. Unfortunately, only Line 301was processed by Star, with FORGE personnel performing minimal processing on Line 302. The quality of the migration of the 3D data by Star was not high. However, the unmigrated version of the 3D data was of sufficient quality to interpret the alluvial basement reflection. The unmigrated data indicate that the granite surface is continuous and undulatory and lacking in any evidence of subvertical fault offsets beneath the FORGE site (Miller and Allis, 2018, Miller et al., 2018, Miller et al., 2019, Hardwick et al., 2019, Simmons et al., 2019).

Because the initial efforts as described above were incomplete, it was decided to have the new 3D and legacy 2D data reprocessed using state of the art techniques. The goal of the reprocessing was to further refine the seismic interpretation for improved imaging of the valley fill-granite contact, and of the deposits above the granite basement. Special attention was paid to the prestack removal of noise such as ground roll and any other noise identified by testing. In addition, depth imaging was performed.

An invitation to bid on reprocessing the Utah FORGE data was issued in August, 2018. The bid was awarded to Land Seismic Noise Specialists (LSNS) of Denver, Colorado, in September. 2018. The LSNS bid proposed a plan to analyze and remove the noise present in the data and to perform all requested reprocessing and depth imaging. The data were delivered to LSNS on September 15, 2018, with the expectation that the work would be completed by December 31, 2018.

This report describes LSNS efforts up to and including delivering the processed data for interpretation. A complete list of products that were delivered is given elsewhere in this report.

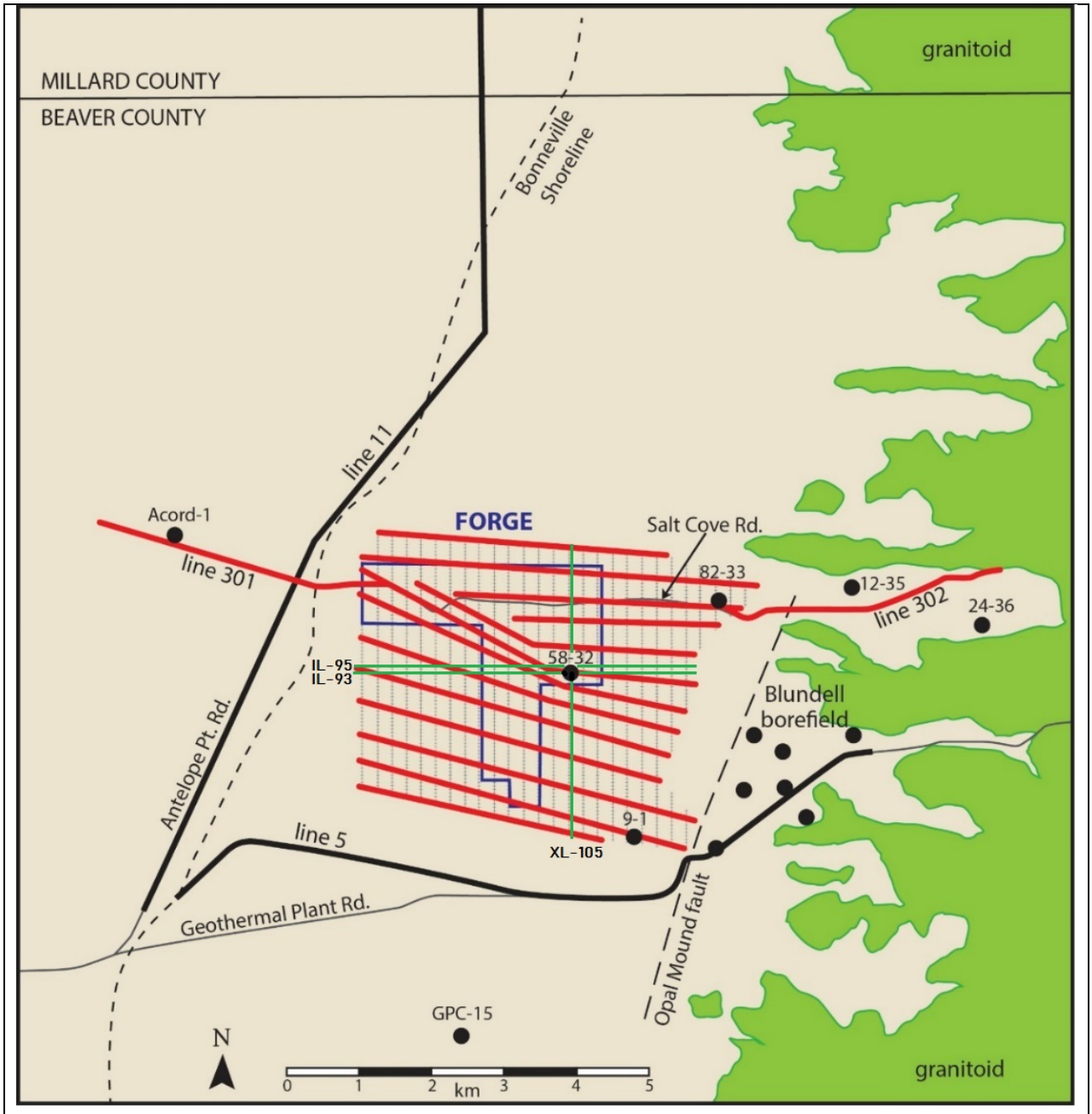

Figure 1: Seismic survey profile locations. The 3D survey area comprises 13 red source lines (vibrator point locations 50 m apart), and 27 gray geophone lines geophone locations (oriented N-S, geophone interval 50 m). Red lines 301 and 302 are new 2D seismic lines; heavy black lines labeled 5 and 11 are legacy 2D lines licensed from Seismic Exchange, Inc. After Miller et al. (2019). Green lines are 3D inlines (IL) and crosslines (XL) discussed in this report.

Review of 3D and 2D Recording.

As explained in Miller et al. (2019), the new 3D data were recorded using 1,114 source points and 1,741 receiver points in the 3-D area. Receivers were located at 50-m intervals and source points were energized at 50-m intervals (Figures 1 and 2). All receivers were active for each source point. The 3D data were organized geometrically into CDP bins spaced 25 m apart and were further organized into 170 "inlines" oriented west-east and 213 "crosslines" oriented south-north (details in Figure 2). The two new 4-kilometer-long 2-D seismic lines (301 and 302) extend east and west from the 3-D survey area and consist of 161 receiver locations with source points at each receiver, except for points that were close to pipelines or other hazards (Figure 1). These new 2D data were organized into Common Depth Point (CDP) bins along each line, spaced 12.5 m apart. The energy source used for both the new 2D and 3D surveys was a Vibroseis method consisting of two I/O AHV IV 364 and 365 vibrators spaced 30 feet apart. Each vibrator imparts 62,000 lbs. of peak force and was operated at 70% of peak force. The Vibroseis sweep produced a 4-48 Hz linear excitation that was 12 seconds in duration with four sweeps per source location. Legacy 2D Lines 5 and 11 were recorded in 1979 and are oriented roughly south-north along Antelope Pt. Rd., and oriented east-west near Geothermal Plant Rd. (Figure 1).

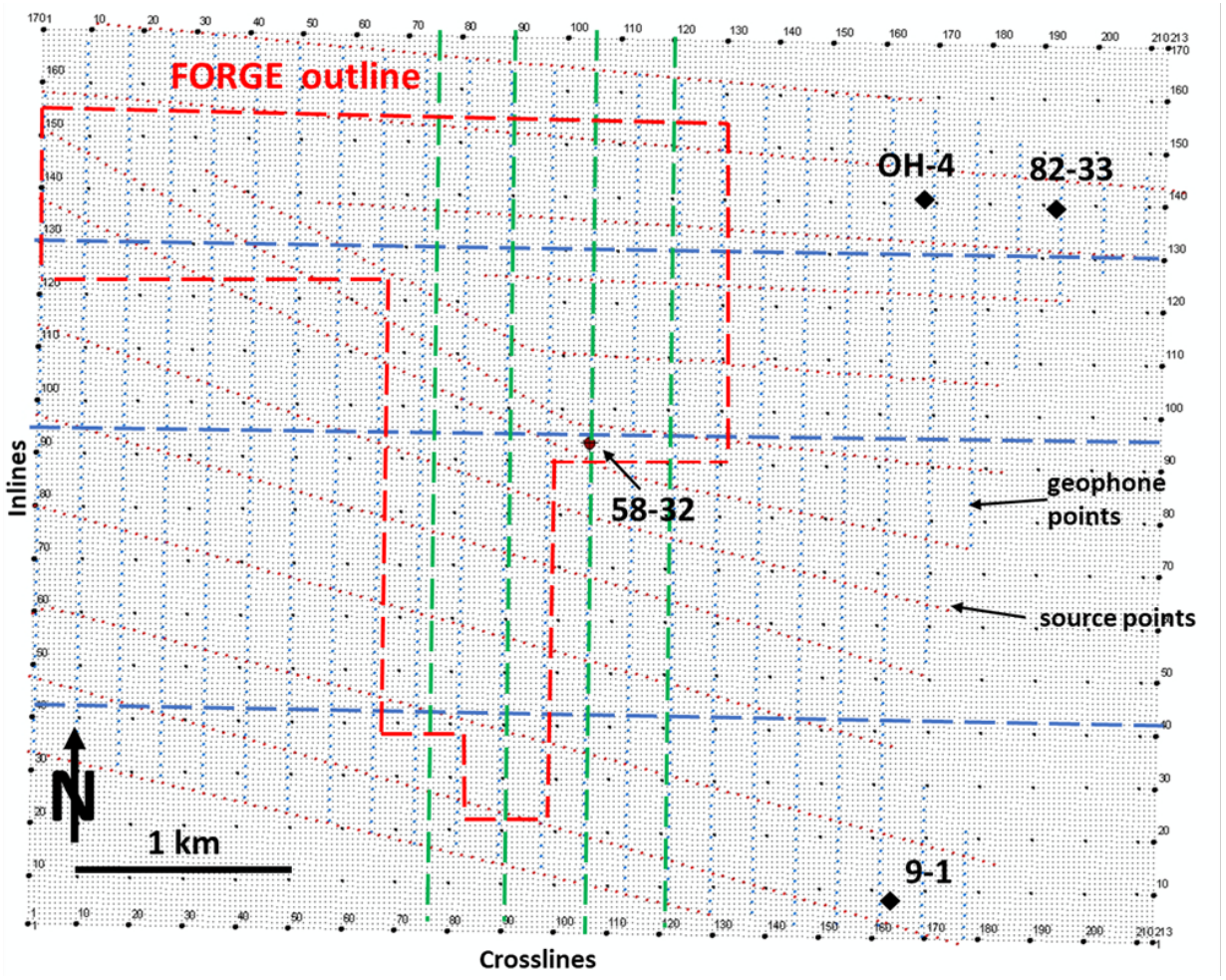

Figure 2. Details of the source and receiver points, the Utah FORGE boundary (red dashes), north-south crosslines (green dashes) and west-east inlines (blue dashes) are lines chosen for discussion in Miller et al. (2019). Well 58-32 is the FORGE well drilled during 2017, and wells 9-1, 82-33, and OH-4 are exploration wells drilled in the late 1970s that penetrated granitic bedrock. CDP bins as well as inline and crossline numbering system are displayed around the perimeter of the figure. After Miller et al. (2019).

Horizontal Limits of 3D and 2D Survey Coverage.

In a 3D seismic survey, the full areal extent of the survey may not necessarily be valid for interpretation. The reason for this is twofold and both are referred to as "edge effects". First, for each CDP bin, it is desirable to have traces with a large distribution of source-receiver offsets, i.e. traces whose source-receiver offset is small (sometimes coincident) and those that have a large offset, referred to as high fold. High fold facilitates accurate velocity determination and provides a good signal to noise ratio (*Schlumberger, 2019a).* Second, the migration process, which attempts to accurately position the reflections in space, usually requires reflected energy from all directions about each CDP bin (*Schlumberger, 2019b)*. Neither of these two conditions is met at the edges of the survey. At the edges there are few traces contributing to the CDP bins (low fold), and there are naturally no traces outside the edges of the survey. The migration edge effects which are sometimes referred to as migration artifacts, manifest as upwardly curved events.

Figure 3 shows the relative fold distribution for the FORGE 3D survey. Dark blue indicates CDP bins with the lowest fold (and a limited range of source-receiver offsets); red indicates CDP bins with the highest fold and largest possible distribution of source-receiver offsets. The white square in the center of the figure indicates generally where the interpretations will be most valid; Outside of this white square, the data may be contaminated by edge effects and interpreters should exercise caution when making geological interpretations. Figure 4 shows the edge effect on the southern end of crossline XL-105. These upwardly turned reflections are primarily a migration edge effect (artifact), but are partially due to low fold as well.

Figure 5 illustrates edge effects on inline IL-95. The top is an unmigrated time section and lacks coherent reflections on the west end of the line, possibly because of low fold in that area. The east end is an example of low fold as the line approaches the edge of the survey, but signal from the granite reflector is strong to the edge of the survey. The green vertical line indicates the eastern extent of shallow surface coverage. The bottom shows edge effects on both the east and west ends of the line. The west end has upturned energy which is an artifact of migration where there is little to no signal and should be considered invalid. However, the east end shows the granite reflection extending to the east of the green line. This phenomena is also an edge effect but can be considered valid information. The migration process will necessarily move a dipping reflector toward the updip direction and, because the granite reflection is so strong in this area, it can be interpreted as valid information. However, the deeper energy is a migration edge effect because there is no coherent energy in that area on A, above.

Migration edge effects are also present on the new 2D data but are much less severe. The reason for this is that these lines utilized a regular recording configuration, i.e. there was a source point coincident at every receiver point. This configuration causes a linear fold reduction at the end of each line and also insures that there is shallow energy recorded to the end of each line, greatly reducing migration edge effects.

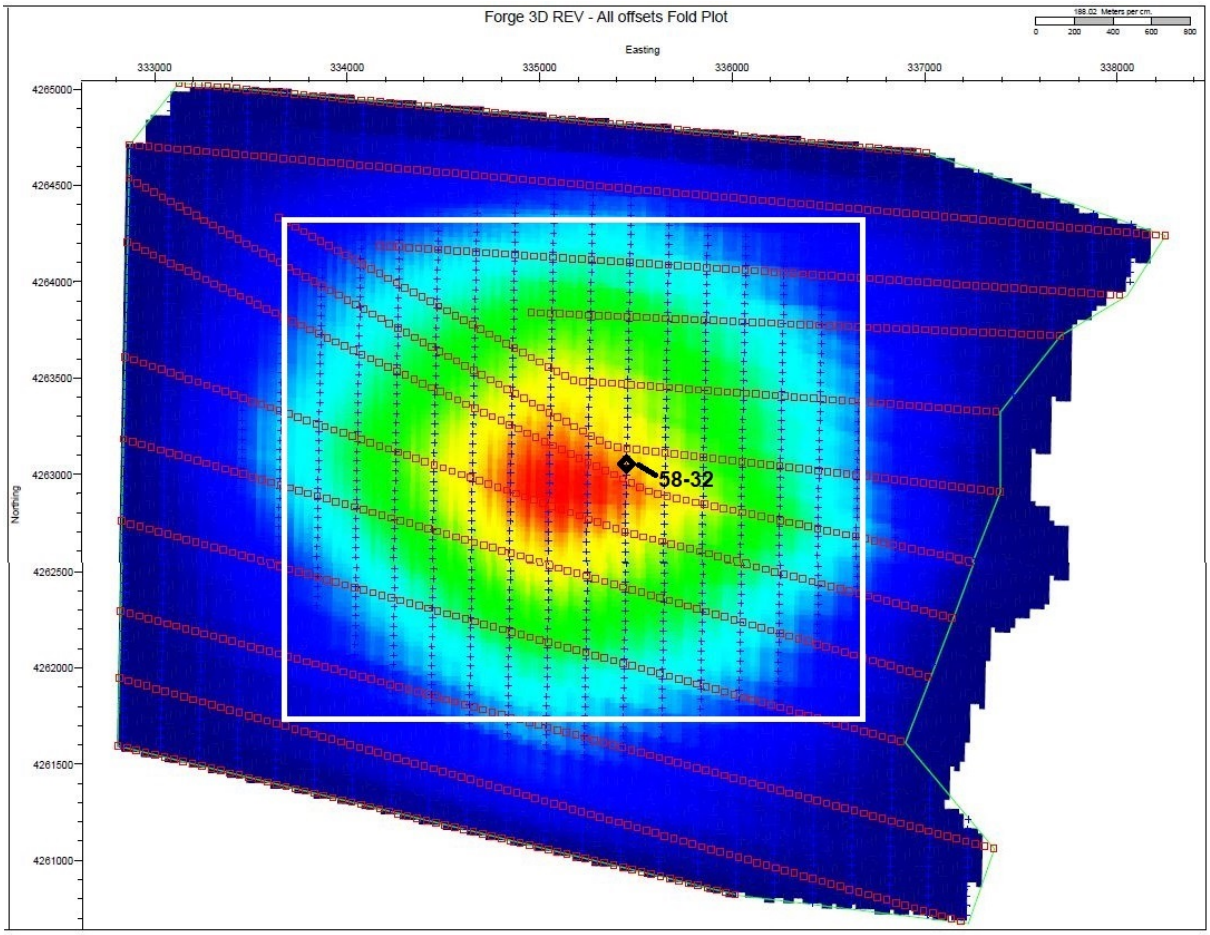

Figure 3. Diagram indicating relative minimum and maximum seismic fold (number of traces contributing to a CDP bin) based on the 3D recording configuration. Blue = Minimum fold; Red = maximum fold. White box indicates the general area where the 3D data should not be affected by edge effects of low fold and migration artifacts. Care should be taken when interpreting data outside of this box.

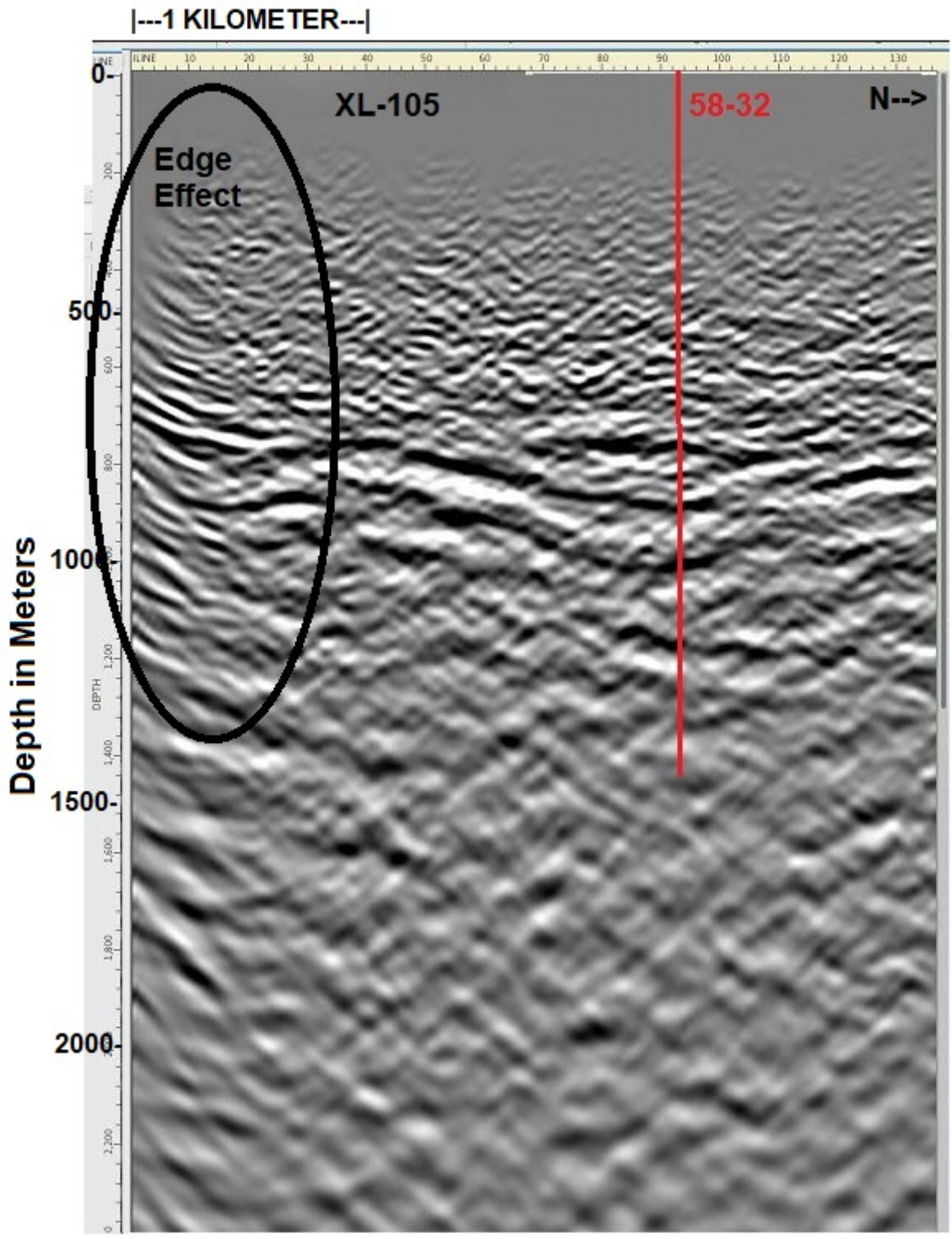

Figure 4. North-south crossline 105 (XL-105) intersecting test well 58-32 indicating the 3D "edge effect" at the southern end of the line. This effect arises from the low fold and the migration process (migration artifact) and should not be considered valid information.

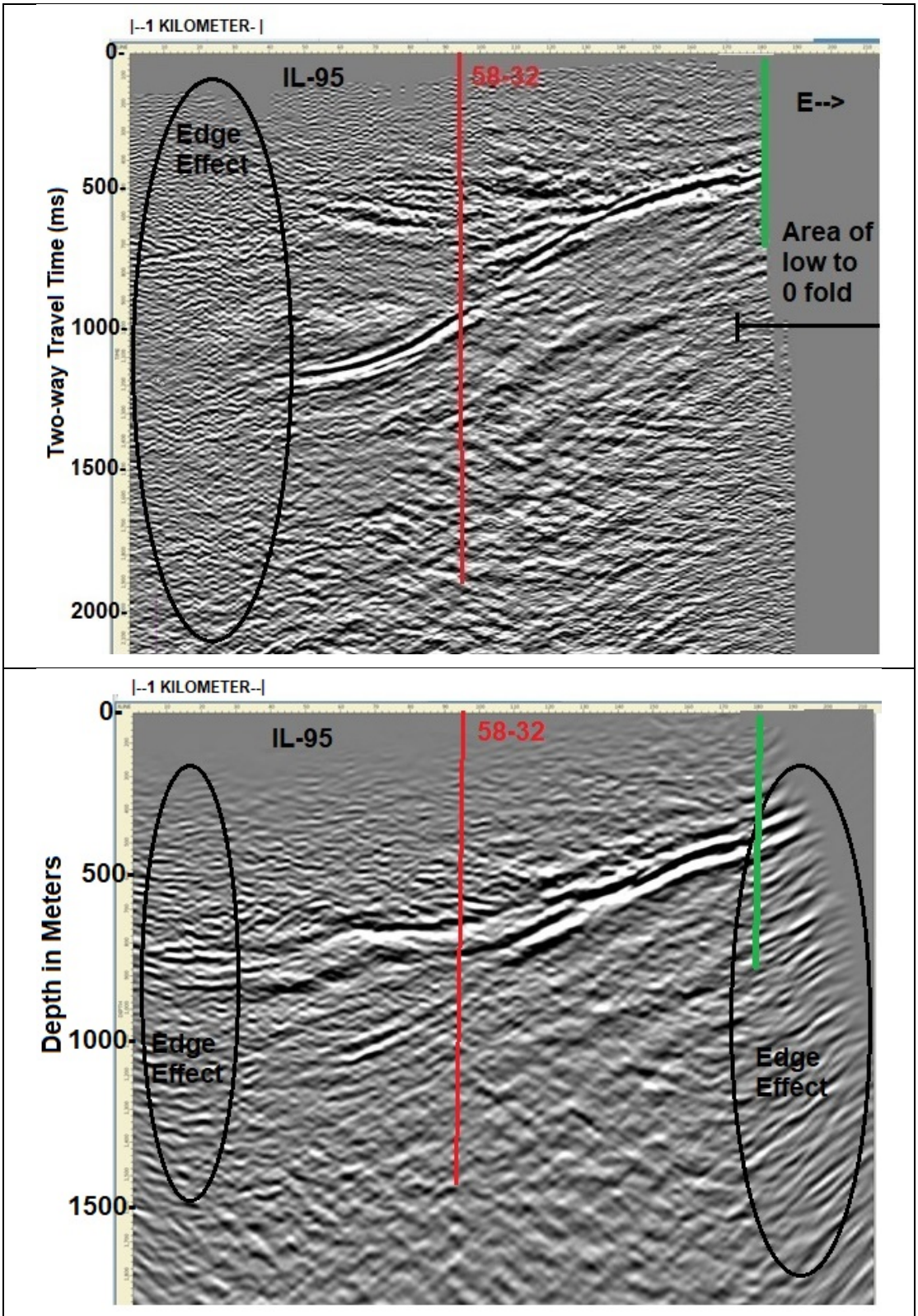

Figure 5. Top: Unmigrated time shows lack of reflections on the west, possibly because of low fold; also indicated is low fold on the east end. Vertical green line indicates eastern extent of shallow surface coverage. Bottom: Migrated depth of A. Migration edge effects can be seen on the west end. The granite reflection has migrated east of the green line which is valid. Migration artifacts are deeper.

Comparison of Processing Flows utilized by LSNS and Star Geophysics, Inc.

Table 1 gives a comparison of the processing flow used by LSNS compared with that of Star Geophysics, Inc. The following are the significant differences in the two processing flows:

- LSNS performed two passes of noise attenuation (Table 1, steps 3 and 7) whereas Star's attempt at noise removal was unsuccessful.
- Both companies applied refraction statics and deconvolution, but in a different order.
- Star applied a process called "trim statics" at step 8. This process is a method by which reflected energy between traces is "forced" to line up in a coherent manner, independent of the geology. It is a process that is sometimes necessary when data contains excessive noise, and its application may be indicate that Star was unable to achieve precise noise removal.
- The lack of trim statics in the LSNS flow indicates that random and coherent noise was successfully identified and removed.
- Star's 3D processing ended at their unmigrated stack subsequently followed by depth conversion.
- LSNS performed both prestack time and prestack depth migration.

Table 1: Generalized Processing flow performed by LSNS compared with Star Geophysics, Inc. Complete details of Star's processing can be found in Miller and Allis (2018).

Step	Land Seismic Noise Specialists (All 3D and 2D data)	Star Geophysics, Inc. (3D and 2D Line 301 only)
1	Geometry corrections, QC Trace edits, and refraction statics calculation and application	Geometry corrections
2	Amplitude balancing	Gain Recovery and trace amplitude equalization
3	Pre-deconvolution noise attenuation: airblast denoise, spectral edit denoise, proprietary LSNS denoise	Attempted noise removal failed.
4		Bandpass Filter & Surface Consistent Spiking Deconvolution
5		Refraction Statics
6	Iterative velocity and residual statics analysis (2 passes)	Iterative velocity and residual statics analysis
7	Spiking Deconvolution (180ms filter) and post-deconvolution noise attenuation – spectral edit and despike	
8		Trim Statics
9	Offset bin interpolation (3D only)	5D Offset bin interpolation (3D only)
10		Stacking Velocity Analysis
11		CDP Stacking and post stack scaling
12	CDP Stacking and post stack enhancements	Depth Conversion (3D only)
13		Post Stack time migration (2D Line 301 only)
13	Pre-stack time migration velocity analysis on migrated gathers	
14	Pre-stack time migration and post-stack enhancements	
15	Pre-stack depth migration velocity analysis and model building	
16	Pre-stack depth migration using an estimated anisotropic velocity model and post-stack enhancements	
17	Bandpass Filter (4-8-80-120 hz)	

Details of LSNS reprocessing

LSNS began processing the data in late September, 2018. Time processing began on the new 3D survey, Line 301 and 302. Two problems were immediately encountered. First was difficulty in creating a refraction statics solution, a process that compensates for lateral variations in near surface velocity. Unusually large variations in near surface velocity were encountered in the Utah FORGE area, but refraction statics solutions were eventually obtained. Second, severe random and coherent noise issues were encountered. Although this was expected, it took much longer to solve the noise problems than was originally anticipated. LSNS used proprietary software which uses a machine learning denoise algorithm to search for consistent and repeatable noise patterns in the shot and receiver domains of the data and removes them (LSNS, written communication). It was also determined that velocities of the sediments above the top of granite in the study area were directionally dependent, i.e. the velocity needed to create a correct subsurface image was sometimes different depending upon the azimuth between the source and receiver. For example, a common reflection point might be imaged by numerous combinations of sources and receivers. In some cases the velocity needed to image that reflection point would be significantly different if the azimuth between source and receiver was 90 degree (east-west) vs. an azimuth of 180 degrees (north-south) and similarly for other azimuths. This phenomenon required extensive testing in order to estimate the velocity field.

Except for 2D Line 302, the datum of all data presented in this report is 1,800m asl. Because the surface elevations of Line 302 are much higher than 1,800m, a datum of 2,100m asl was used for this line.

3D processing

A comparison of the original processing by Star Geophysics and the new processing by LSNS, is given in Figure 6. This is an unmigrated time version of 3D inline IL-95 which passes 50m north of test well 58-32. Because we did not receive a migrated version of the 3D survey from Star, a comparison of unmigrated time processing is the only direct comparison that can be made. The original processing shown at the top exhibits problems that have been resolved by the new processing (bottom). The yellow oval marked A indicates poorly resolved alluvial sediments; the yellow oval marked B indicates some type of coherent noise and possibly multiple reflections. There is a curious lack of any reflective energy above the horizontal line at approximately 550 ms. The new processing is a better product in all respects, and especially so in resolving the granite reflection to the eastern end of the survey.

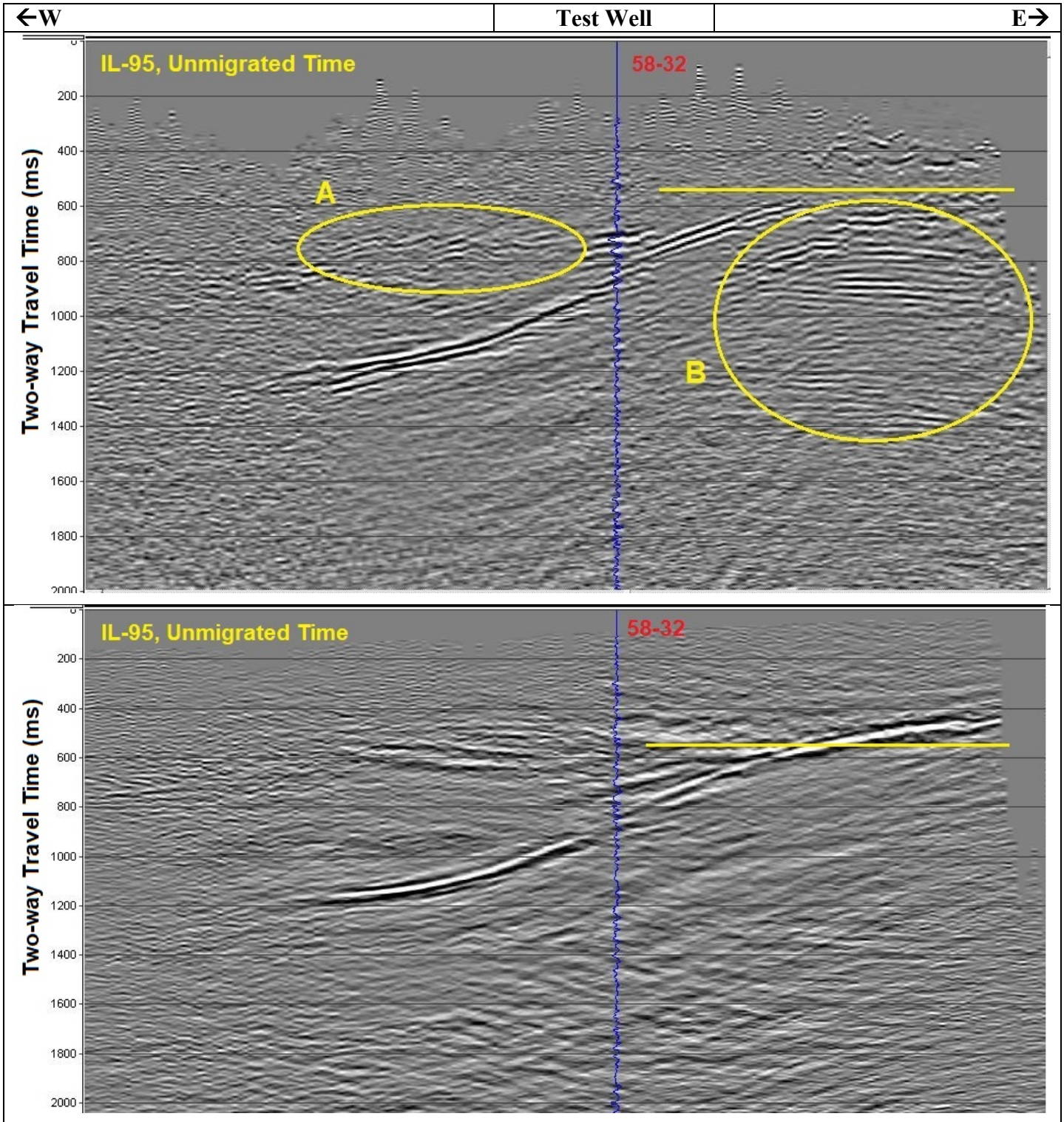

Figure 6. Direct comparison of unmigrated time processing.
Top: Star Geophysics product. Yellow oval labeled A indicates poorly resolved alluvial sediments; yellow oval marked B indicates coherent noise and possibly multiples. All reflections appear to disappear above the horizontal line, including that of the granite. Bottom: LSNS result. Sediments are better resolved, coherent noise and multiples are eliminated. There is reflective energy above the yellow line including the granite reflection which extends to the east end of the line. The projected location of test well 58-32 is shown in blue.

Subsequent to creating the unmigrated time volume, both prestack time and prestack depth migration were performed. A considerable amount of time was spent determining the optimum velocity model for migration. The velocity model determined directly from the seismic data was highly azimuth-dependent, meaning the velocity field changed depending on the azimuth between the source and receiver (horizontal anisotropy). It is surmised from this anisotropy that there was non-uniform sedimentation processes during basin evolution, but this cannot be stated conclusively without additional well data.

Unfortunately, it was not possible to fully account for this horizontal anisotropy (parameter epsilon) when migrating this data set because longer source-receiver offsets and additional well data were needed. However, a migration algorithm that used an estimated anisotropy parameter in the vertical direction (parameter delta) was shown to migrate the depth of the granite interface on the seismic data to that of test well 58-32. The delta parameter also affects the migration raypaths and thus has a horizontal effect. The improved imaging away from the well using this method, as opposed to the standard (delta=0) migration method, gives further confidence that the parameter used, and the imaging result, is correct (LSNS, written communication).

Figures 7 and 8 give a comparison of the 3D processing progression using inline IL-93 which intersects test well 58-32. This line is 50m south of IL-95 shown in Figure 6 and has a similar appearance. Figure 7, top, shows the unmigrated time section of IL-93 and Figure 7, bottom, shows the prestack migrated time version. The time sections indicate that the granite reflection is laterally continuous, with no vertical offsets within the resolution of the seismic data (refer below for a discussion of the limits of vertical resolution). Another indication of vertical offset would be diffracted energy in the unmigrated version (Figure 7, top) and no diffractions are seen.

Figure 8 shows the prestack depth migration of IL-93 using the estimated anisotropic migration; uninterpreted (top) and interpreted by the author (bottom). Again, the top of granite reflection is interpreted to be continuous. The depth at test well 58-32 is indicated by the horizontal amber line. This depth corresponds well with the granite depth as determined by logs and cuttings in well 58-32. The reader is reminded that the datum of this line is 1,800m asl. The surface elevation at well 58-32 is 1,685m asl.

The question of how much vertical offset in the top-of-granite surface can be detected using the reflection seismic method can be answered using the ¼ wavelength principle (Yilmaz, 2001). This principle states that the minimum offset that can be detected is approximately ¼ of the dominant frequency of the seismic wavelet. In this survey, the dominant frequency of the data is 30 Hz (f) and the velocity immediately above the top of granite is 3000 m/s (v). Therefore, the wavelength, v/f, is 100 m. So, using the ¼ wavelength principle we can expect to detect offsets in the granite reflector of 25m or greater. This principle is a function of the recording process and the earth properties, and thus in principle applies both to the STAR and LSNS processing. However, the domain over which this best resolution pertains is significantly greater for the LSNS results due to superior noise removal and velocity estimation.

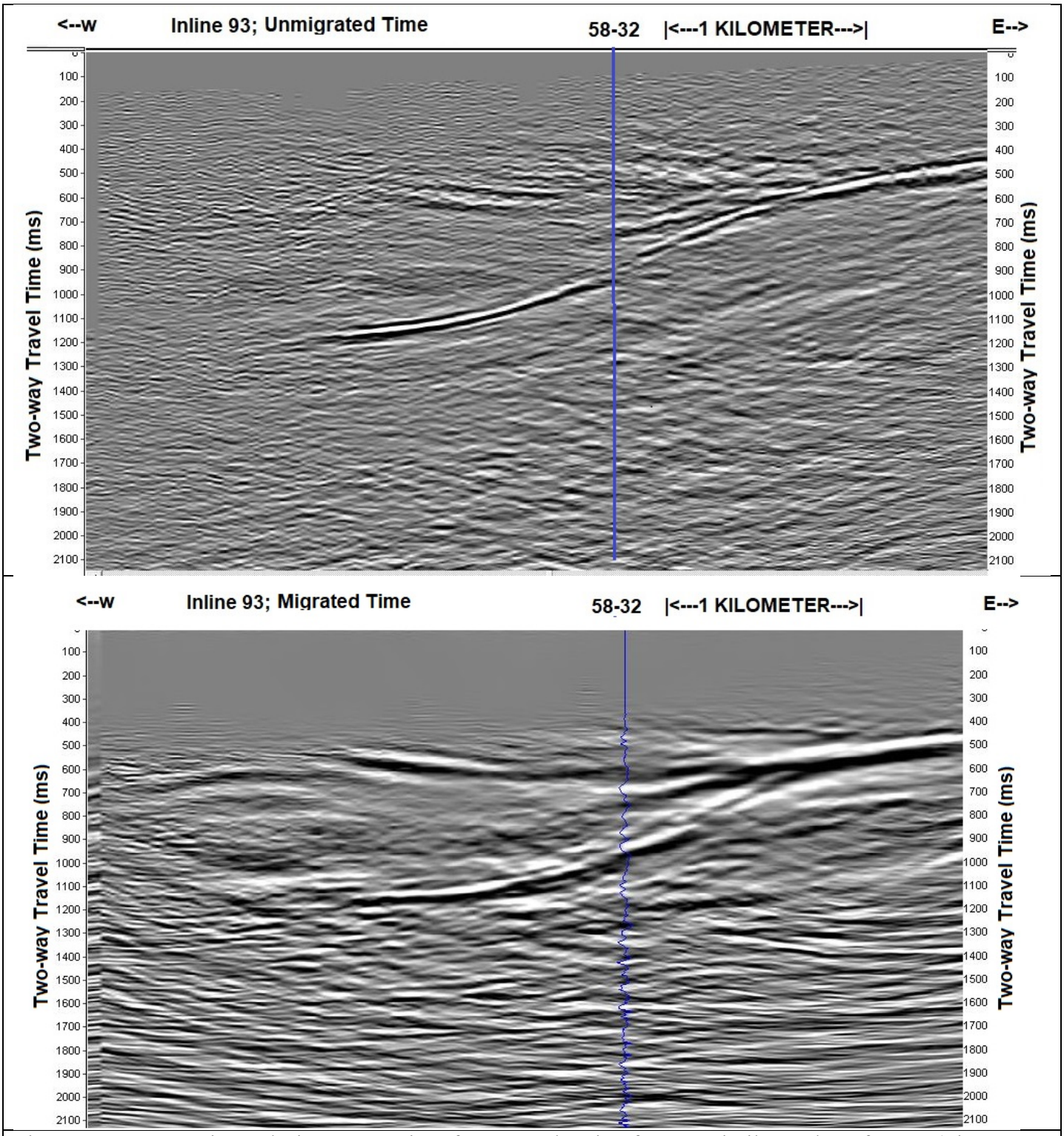

Figure 7. Top: Unmigrated Time processing; for IL-93 showing features similar to that of IL-95 (Figure 6, bottom). This line is 50m south of IL-95. Bottom: Migrated time version of top, showing a horizontally continuous reflection from the top of granite with no significant vertical offset. The location of test well 58-32 is shown in blue.

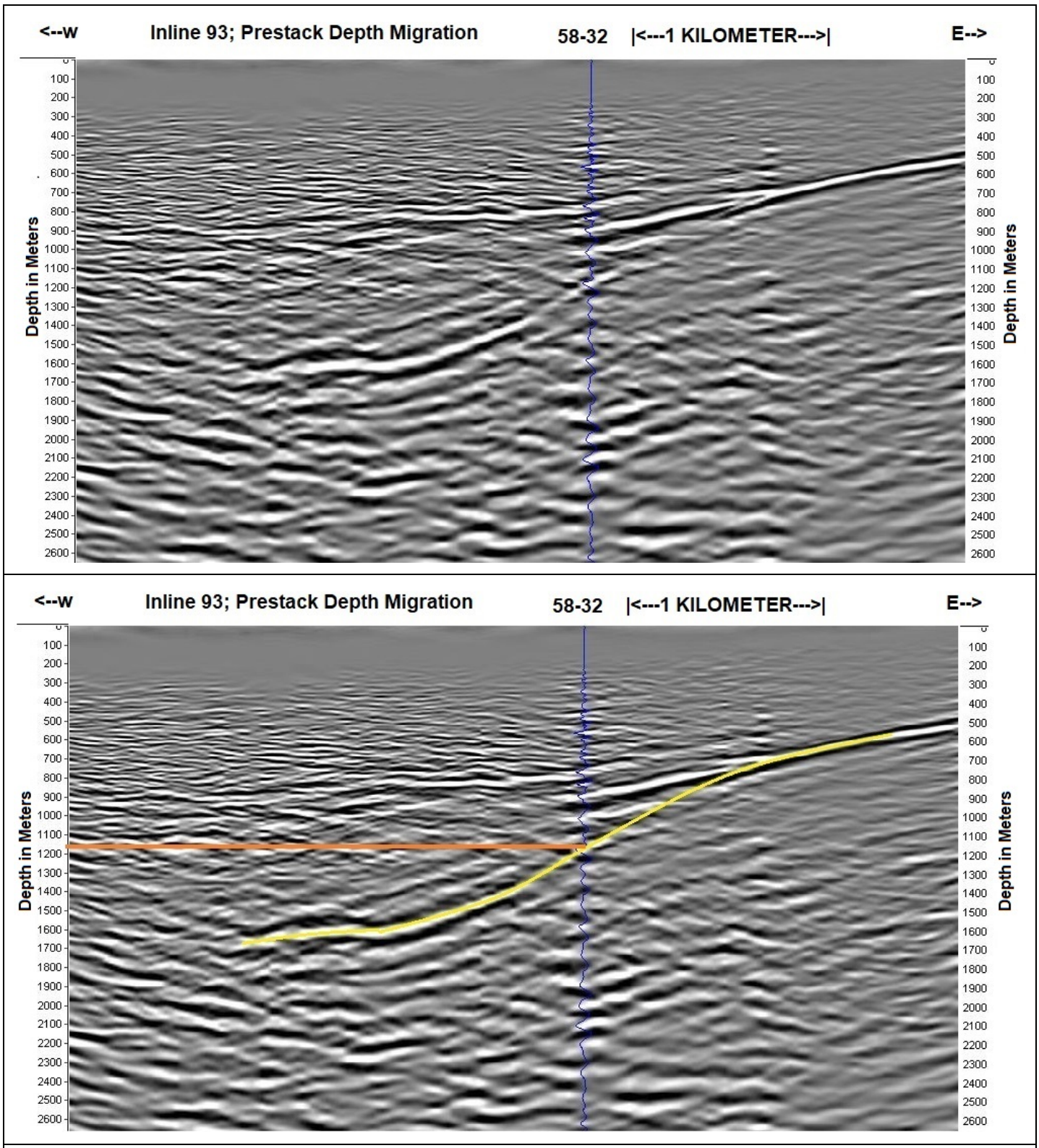

Figure 8. Top: Uninterpreted estimated anisotropic prestack depth migration. Bottom: Interpreted version of the top. Yellow line indicates the author's interpretation of the top of granite reflector. The horizontal amber line indicates the depth to top-of-granite at test well 58-32. This depth corresponds well with the depth of granite from logs and cuttings in well 58-32. The location of test well 58-32 is shown in blue.

2D Processing

Four 2D lines were processed by LSNS; Lines 301 and 30, recorded in 2017 and lines 5 and 11, proprietary lines licensed by Utah FORGE in late 2017 from SEI. In Phase 2C, only lines 301 and 302 were processed from the field data. Lines 5 and 11 were processed by SEIMAX Technologies, a processing company contracted by SEI, and digital time sections were provided to Utah FORGE. These two lines were converted to depth by FORGE Utah personnel using well data and velocities provided by SEI (Miller and Allis, 2018).

The generalized processing flow is given in Table 1.

2D Line 302

2D Line 302 was recorded along Salt Cove Road in 2017 and extends 4 kilometers east from the 3D survey data area (Figure 1). This line images the shallow reflection from the top of granite. As stated in the introduction, Utah FORGE personnel had minimally processed this line and it appeared that the granite formed a shallow basin. However, LSNS applied the refraction statics process to this line, a process that compensates for near-surface velocity variations, and the result was a significant improvement: the basin proved to be an artifact of this near surface velocity variation. Figure 9 illustrates the improvement. The top is the unmigrated time section processed by Utah FORGE personnel. The bottom is the LSNS version of the unmigrated time section after application of refraction statics. LSNS continued processing this line to the point of prestack depth migration (not shown).

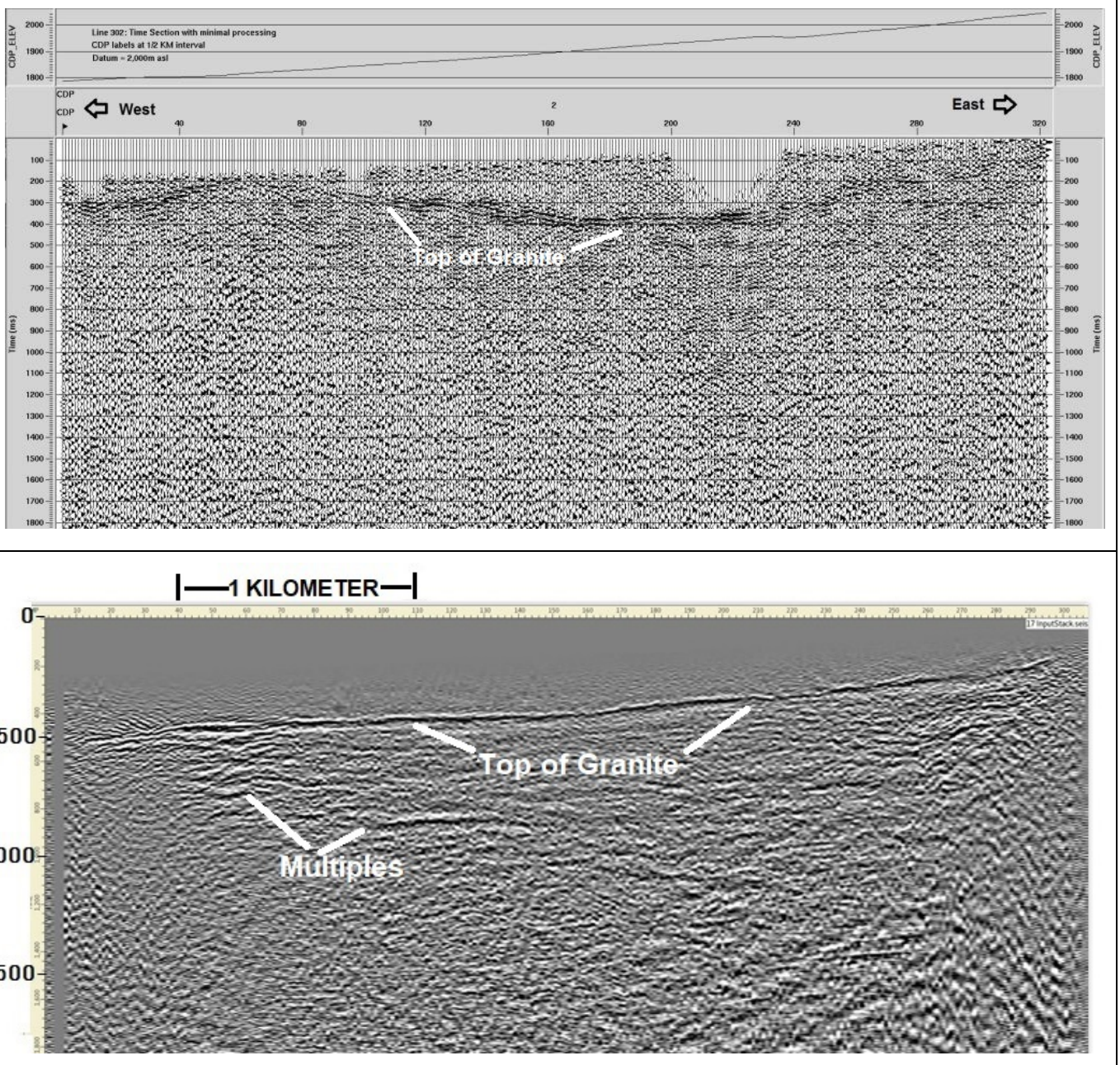

Figure 9. 2D Line 302. Top: Unmigrated time after minimal processing by Utah FORGE personnel. Bottom: Unmigrated time after processing by LSNS using refraction statics showing that the shallow basin is an artifact of near surface lateral velocity variations. Note: the datum of LSNS processing is 2100m asl; 100m above that of Utah FORGE's processing.

2D Line 301

2D Line 301 was recorded along Salt Cove Road in 2017 and extends 4 kilometers west from the 3D survey (Figure 1). Star Geophysics provided a prestack time migrated version of this line and Utah FORGE personnel converted this version to depth using well velocities and tie velocities from its tie point with Legacy Line 11 (Miller and Allis, 2018). LSNS provided a prestack depth migrated version of this line. Figure 10 shows the Star processing (top) compared with the LSNS prestack depth migration processing (bottom). Above 1500m the two versions are similar, but below that depth the LSNS processing shows much greater reflectivity and has reflections dipping up and to the east on the east end which should be expected as the line approaches the 3D survey.

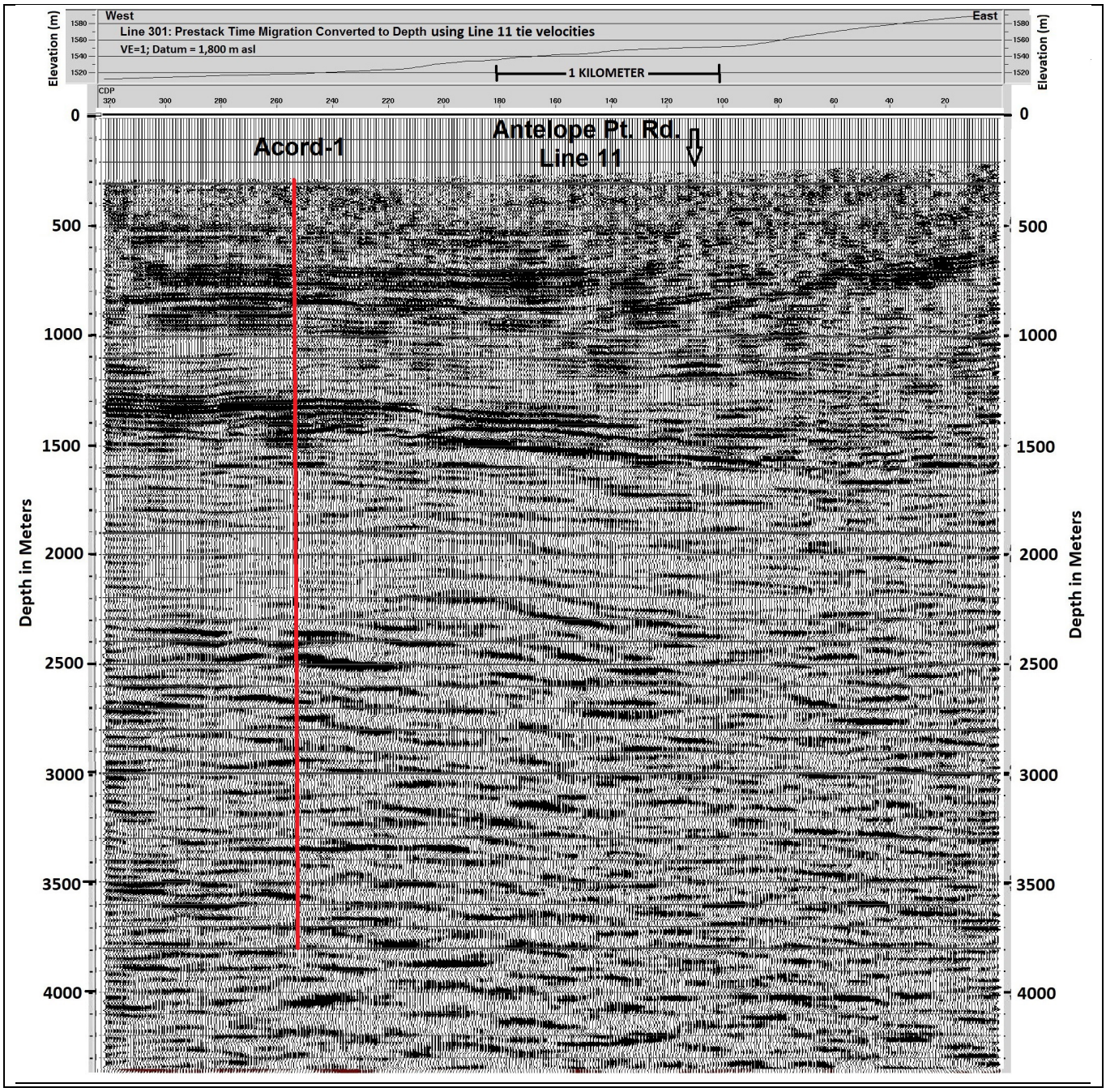
West
East
Line 301: Prestack Time Migration Converted to Depth using Line 11 tie velocities
VE=1; Datum = 1,800 m asl
1 KILOMETER
Elevation (m)
CDP
Acord-1
Antelope Pt. Rd.
Line 11
Depth in Meters

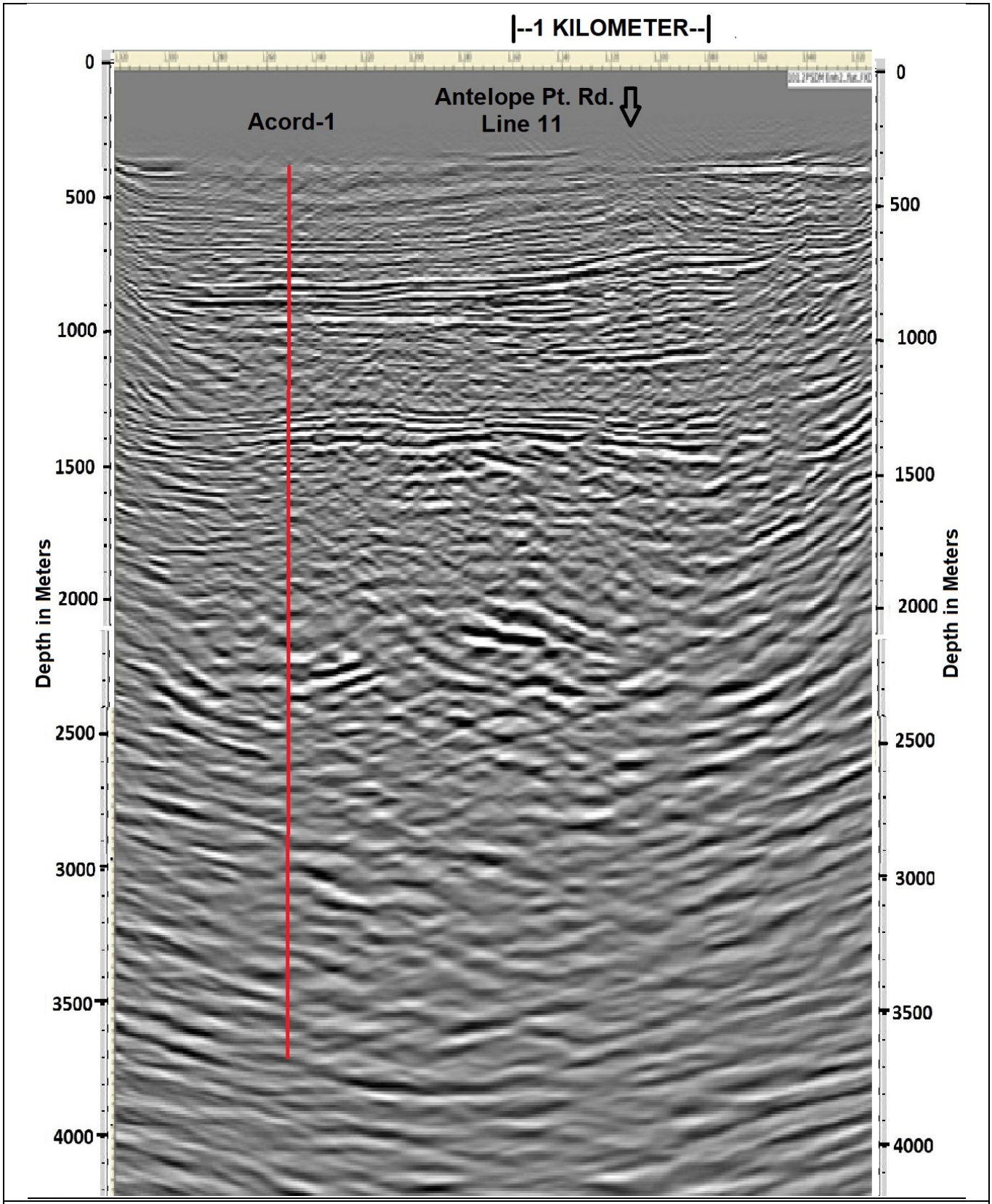

Figure 10: Top: 2D Line 301 processed by Star through prestack time migration; converted to depth by Utah FORGE personnel (after Miller and Allis, 2018). Bottom: Version processed by LSNS through prestack depth migration. LSNS processing shows greater reflectivity below 1500m and reflections dipping up and to the east going into the 3D survey, which should be expected). Location of Acord-1 exploration well and tie point with Legacy Line 11 at Antelope Point Road are indicated.

2D Legacy Line 5

2D Line 5 was recorded in 1978 along and near geothermal plant road, south of the Utah FORGE 3D survey (Figure 1). Among all of the 2D lines, this line proved to be the most difficult to image. The line was initially processed in 1979 by the company that recorded the data; it was reprocessed in 2016 by SEIMAX Technologies, a processing company under contract to SEI. Only a Tiff image of the 1979 processing was available. We identified a company to convert that image to SEG-Y digital traces. Utah FORGE personnel converted that image to depth using a combination of velocities from well 58-32 and well 9-1, projected onto the line's location (Figure 1, Miller and Allis, 2018). Figure 11, top, shows the result. The 2016 reprocessing did not resolve the granite reflection nearly as well as the 1979 processing and that result is shown in Figure 11, bottom. The granite reflection is faint and subhorizontal reflections are poorly resolved relative to the 1979 processing.

LSNS also encountered difficulty imaging the top of granite reflection. However, they were successful in imaging the subhorizontal reflections as laterally continuous and the top of granite can be inferred by the truncations of these reflections as well as a faint dipping reflection. The prestack depth migrated result is shown in Figure 12.

The 1979 processing appears superior to both the 2016 and current reprocessing. The 1979 processing company no longer exists and there is no record of the personnel that did the processing. Both LSNS and Utah FORGE personnel have discussed this discrepancy at length but cannot determine the reason for the apparent fidelity of the 1979 result.

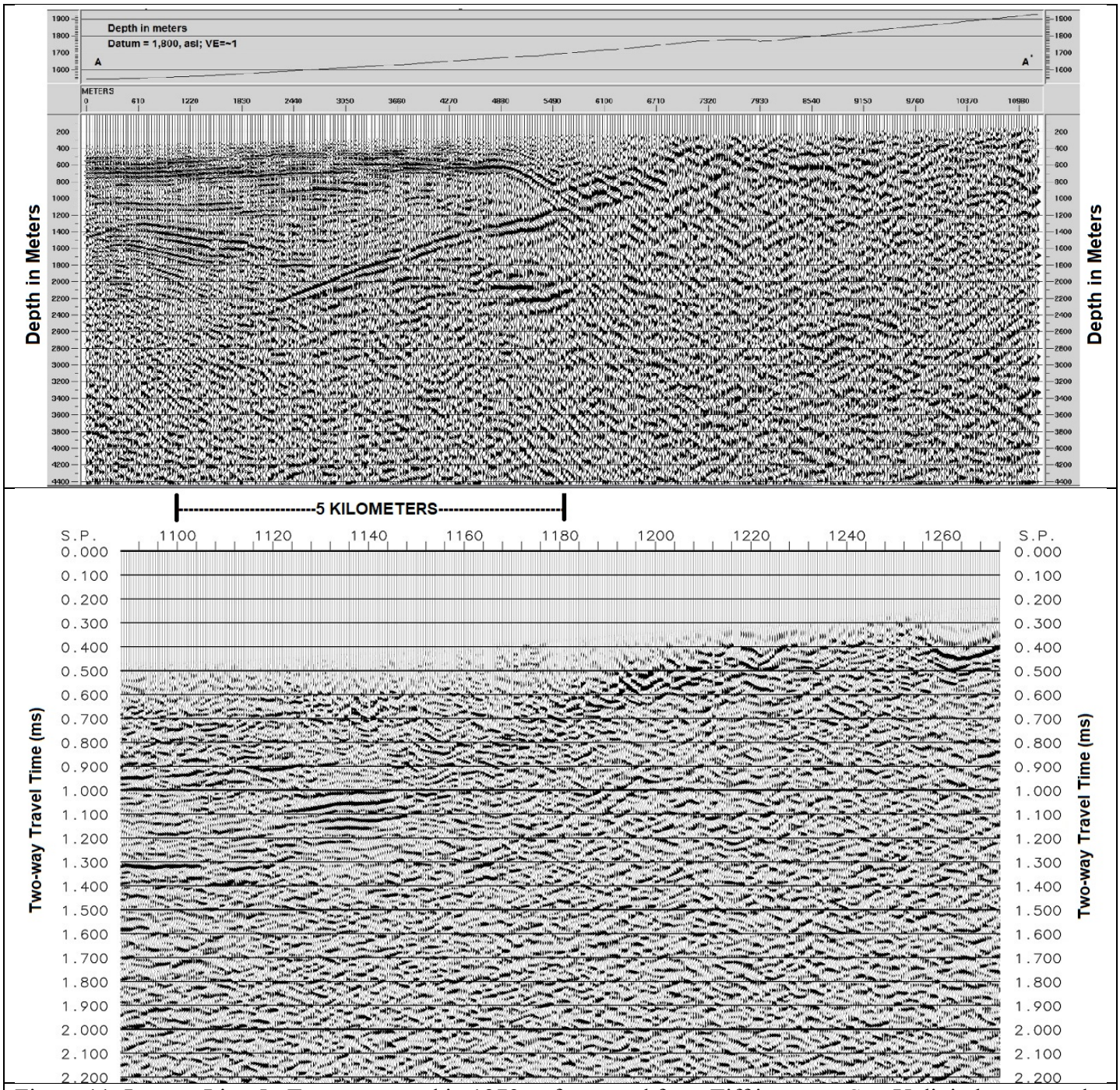

Figure 11: Legacy Line 5. Top: processed in 1979, reformatted from Tiff image to Seg-Y digital traces and converted depth using a combination of velocities from well 58-32 and well 9-1, projected onto the line's location. (after Miller and Allis, 2018). Bottom: reprocessed in 2016 through prestack time migration. The granite reflection is very faint and subhorizontal reflections are poorly resolved.
Seismic data are owned or controlled by Seismic Exchange, Inc.; Interpretation where shown, is that of Utah FORGE.

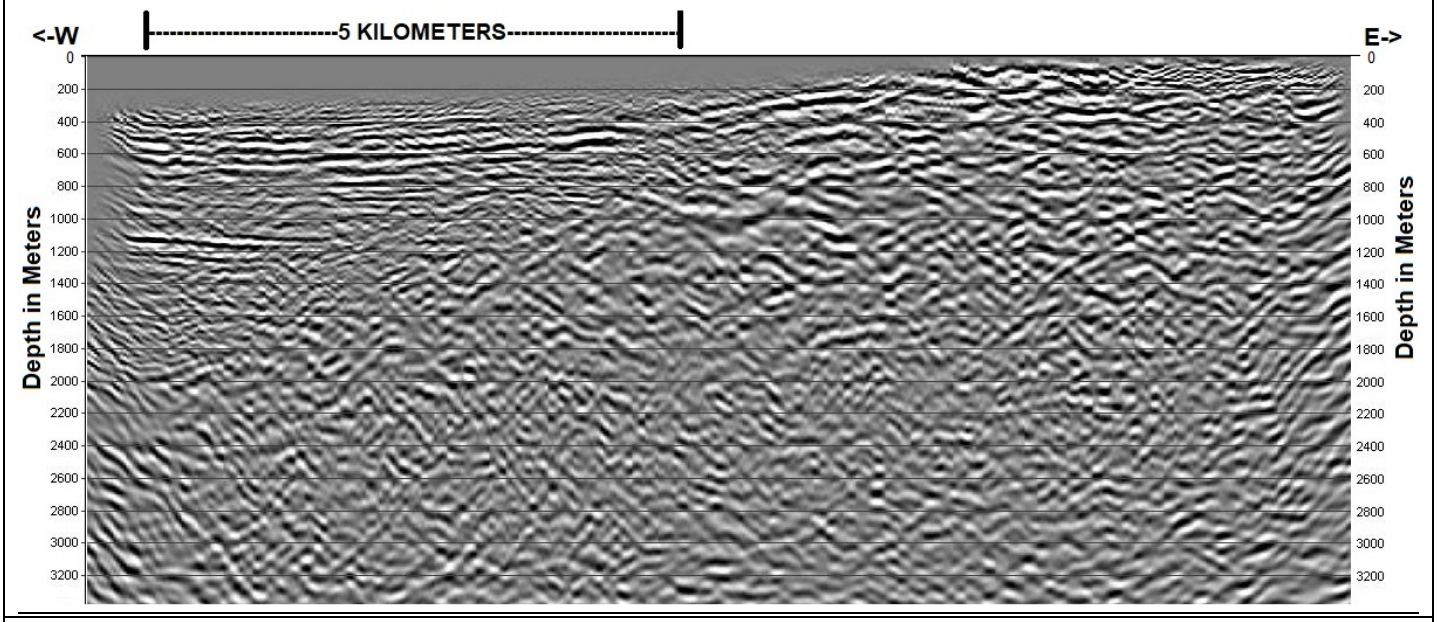

Figure 12: Legacy Line 5. Prestack depth migration by LSNS. Subhorizontal reflections are better resolved than in the 2016 reprocessing shown in Figure 11, bottom.

Seismic data are owned or controlled by Seismic Exchange, Inc.; Interpretation, where shown, is that of Utah FORGE.

2D Legacy Line 11

2D Line 11 was recorded in 1979 along Antelope Point Road, west of the Utah FORGE 3D survey (Figure 1). The line was initially processed in 1979 by the company that recorded the data; it was reprocessed in 2016 by SEIMAX Technologies, a processing company under contract to SEI. In contrast to Line 5, the 2016 processing of Line 11 was far superior to the 1979 processing. Utah FORGE personnel used the prestack time migrated version of the line and converted it to depth using the processing velocities provided by SEI (Figure 13, top). LSNS performed prestack depth migration (Figure 13, bottom). Both processed versions are of high quality. LSNS reported that detailed velocity analysis was required because of large lateral velocity changes. The LSNS processing seems to have resolved the shallow portion of the anticline on the north side of the line as a continuous feature, whereas it appears faulted in the 2016 processing. However, this portion of the line is well north of the Utah FORGE study area.

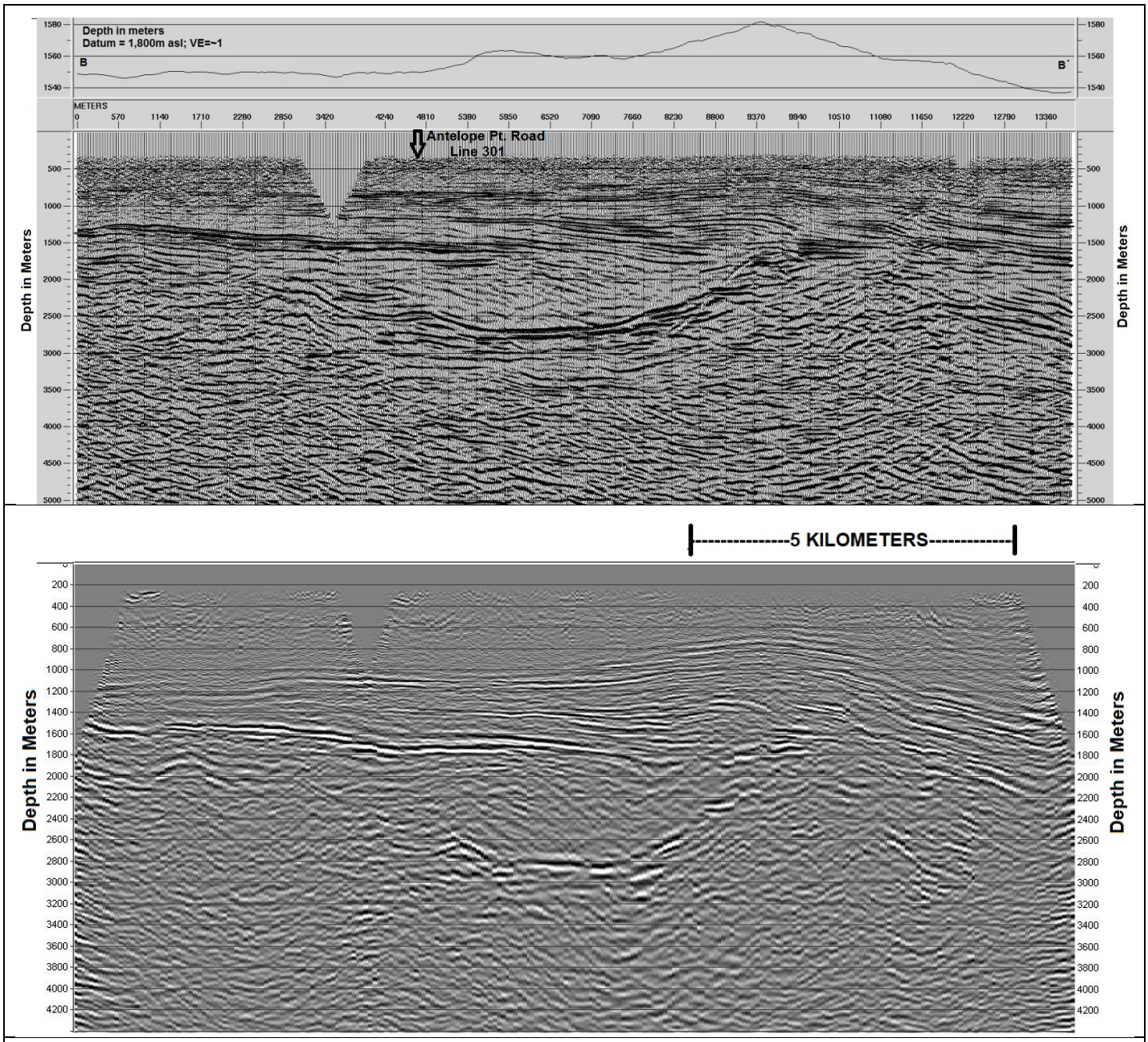

Figure 13. Legacy Line 11. Top: Prestack time migration provided by SEI, converted to depth by Utah FORGE using the processing velocities provided (after Miller and Allis, 2018). Bottom: Prestack depth migration by LSNS. Both versions of the processing are of high quality.

Seismic data are owned or controlled by Seismic Exchange, Inc.; Interpretation, where shown, is that of Utah FORGE.

Deliverable Items Received

As mentioned in the Introduction, reprocessing was necessary because the efforts of Star Geophysics, Inc. were incomplete. Star processed the 3D survey to the point of unmigrated time and depth and 2D Line 301 to the point of pretstack time migration but did not process 2D Line 302. LSNS delivered all required items. Table 1 gives a comparison of the items required of, and subsequently delivered by, both companies.

Table 2. Deliverable products received from LSNS and Star Geophysics, Inc. N/A = Not applicable, i.e. not a required deliverable item.

	Deliverable item	Delivered by LSNS	Delivered by Star	Comments
1	Final unmigrated gathers (without NMO)	Yes	Yes	LSNS delivered 2D Lines 5, 11, 301, 302, and the 3D survey as required.
2	Final RMS velocities	Yes	Yes	
3	Unmigrated time stack	Yes	Yes	
4	Unmigrated time depth	N/A	Yes	
5	Poststack time migrated stack	Yes	Yes #	Star processed the 3D survey and 2D Line 301 as indicated. 2D Line 302 was not processed. # Line 301 only
6	Prestack Time Migrated gathers	Yes	No	
7	Prestack Time Migrated stack	Yes	Yes #	
8	Prestack Time Migrated stack (enhanced)	Yes	No	
9	Final Prestack Time Migration velocities	Yes	No	
10	Prestack Depth Migrated gathers	Yes	No	
11	Prestack Depth migrated stack	Yes	No	
12	Prestack Depth Migrated stack (enhanced)	Yes	No	
13	Final Prestack Depth Migration velocities	Yes	No	
14	Processing flows and parameters	Yes	Yes	
15	Interpretation	N/A	No	
16	Final digital report	Yes	No	

Conclusions

The reflection seismic reprocessing carried out by LSNS provided Utah FORGE with a superior product than previously obtained. LSNS delivered to Utah FORGE all of the items required by the contract between LSNS and Utah FORGE.

All of the reflection data have been processed through prestack depth migration. The newly-reprocessed 3D survey has superior shallow and lateral resolution due to improved noise removal and velocity estimation. 2D Line 301 has increased reflectivity at depth and shows upturned reflections on the east approaching the Utah FORGE site as should be expected; 2D Line 302 shows the granite reflection to be planar and dipping up to the west as opposed to minimal processing by Utah FORGE personnel that indicated it may be a shallow, undulating basin.

Reprocessing of Legacy Lines 5 and 11 generally reproduced the results of the 2016 reprocessing provided by SEI. Reprocessing Legacy Line 5 does not answer the question of why the 1979 processing appears superior to both the reprocessing performed in 2016 and for this project.

References

1. Hardwick, C., Hurlbut, W., and Gwynn, M., 2019, Geophysical surveys of the Milford, Utah, FORGE site—gravity and TEM, *in* Allis, R., and Moore, J.N., editors, Geothermal characteristics of the Roosevelt Hot Springs system and adjacent FORGE EGS site, Milford, Utah: Utah Geological Survey Miscellaneous Publication 169-F, 15 p., https://doi.org/10.34191/MP-169-F.
2. Miller, J.J. and Allis, R., 2018**,** Seismic Reflection Profiling at the FORGE Utah EGS Laboratory, Department of Energy Report, DE-EE0007080, University of Utah.
3. Miller, J.J., Allis, R. and Hardwick, C., 2018, Seismic Reflection Profiling at the FORGE Utah EGS Site, 2018, Geothermal Resources Council (GRC) Transactions, v. 42.
4. Miller, J., Allis, R., and Hardwick, C., 2019, Interpretation of seismic reflection surveys near the FORGE enhanced geothermal systems site, Utah, *in* Allis, R., and Moore, J.N., editors, Geothermal characteristics of the Roosevelt Hot Springs system and adjacent FORGE EGS site, Milford, Utah: Utah Geological Survey Miscellaneous Publication 169-H, 13 p., https://doi.org/10.34191/MP-169-H.
5. Simmons, S.F., Kirby, S., Bartley, R., Allis, A., Kleber, E., Knudsen, T., Miller, J.J., Hardwick, C., Rahilly, K., Fischer, T., Jones, C., and Moore, J., 2019, Update on the Geoscientific Understanding of the Utah FORGE Site, PROCEEDINGS, 44th Workshop on Geothermal Reservoir Engineering Stanford University, Stanford, California, February 11-13, 2019, SGP-TR-214 .
6. Schlumberger online Oilfield Glossary, 2019a, https://www.glossary.oilfield.slb.com/en/Terms/s/stack.aspx
7. Schlumberger online Oilfield Glossary, 2019b https://www.glossary.oilfield.slb.com/Terms/m/migration.aspx
8. Yilmaz, O., 2001, Seismic Data Analysis: Processing, Inversion, and Interpretation of Seismic Data, Society of Exploration Geophysics, 2065p., http://dx.doi.org/10.1190/1.9781560801580

Appendix: Files Delivered to Utah FORGE

The results of the reprocessing were delivered to Utah FORGE using File Transfer Protocol (FTP) in April 2019. All files are in digital form as industry-standard SEG-Y format (Barry and others, 1975). The 3D survey and 2D Lines 301 and 302 are available to the public. Legacy 2D Lines 5 and 11, licensed from Seismic Exchange, Inc., are proprietary and are not available to the public except for the derivative depth images presented in this report.

Table 2 gives a list of all the delivered items. Table A1 gives a list of all the stacked, processed files received from LSNS including 1) unmigrated time, 2) prestack time migration, 3) prestack depth migration, 4) velocities used for migration, 5) exact file names and 6) file sizes. For Legacy Lines 5 and 11, the navigation was defined in feet and so the calculated migration velocities were defined in ft/sec. The initial prestack depth migration file has depth in feet, but a second prestack depth migration with depth in meters and a datum of 1,800m asl was generated in order to be consistent with the other lines. Both files were included with the delivered data. For the 3D survey, there is an enhanced, poststack time migrated file, "Forge3d_Poststack_Time_Migration_FXYDecon_Stack.segy", included with the delivered items.

Table A2 gives a list of all the unstacked, CMP gathers for each line including 1) prestack time migration with Normal Moveout applied, 2) prestack time migration without Normal Moveout applied, and 3) velocities used for migration.

Each SEG-Y format file contains a standard text header, referred to as the EBCDIC header, that describes the contents of the file. Figure A1 gives an example of the text header from the 3D processed file "Forge3d_ANI_PSDM_Stack Enh.segy". This header contains at a minimum:

1. Year recorded and year processed
2. Sample interval and data trace length
3. Navigation coordinate system
4. Datum and datum correction velocity
5. Coordinates of the corners of the survey (3D survey only)
6. processing flow
7. Trace header byte locations for various trace header words, which should be sufficient to load the data into a seismic interpretation system. These are:CMP X, CMP Y, CMP bin elevation and final datum static.

Note that for 3D data, the inline (IL) and crossline (XL) numbers and are two byte integers, located in bytes 9-10 and 13-14, respectively.

Line: Data Type	Size in bytes	File Name
301: PSDM Enhanced	7,785,924	Line_301_PSDM_Enh.segy
301: PSDM UnEnhanced	7,785,924	Line_301_PSDM_UNEnh.segy
301: PSDM Interval Velocities	428,364	Line_301_PSDM_Interval_Velocity.segy
301: Unmigrated Time	5,217,924	Line_301_Unmigrated_Stack.segy
301: PSTM Enhanced	5,217,924	Line_301_PSTM_Stack_Enh.segy
301: PSTM UnEnhanced	5,217,924	Line_301_PSTM_Stack_UnEnh.segy
302: PSDM Enhanced	7,446,508	Line_302_PSDM_Enh.segy
302: PSDM UnEnhanced	7,446,508	Line_302_PSDM_UNEnh.segy
302: PSDM Interval Velocities	357,920	Line_302_PSDM_Interval_Velocity.segy
302: Unmigrated Time	4,990,508	Line_302_Unmigrated_Stack.segy
302: PSTM Enhanced	4,990,508	Line_302_PSTM_Stack_Enh.segy
302: PSTM UnEnhanced	4,990,508	Line_302_PSTM_Stack_UnEnh.segy
L5: PSDM Enhanced (depth in feet)	3,622,716	Line_L5_PSDM_Enh.segy
L5: PSDM Enhanced (depth in meters)	2,147,676	Line_L5_PSDM_Enh_Meters.segy
L5: PSDM UnEnhanced (depth in feet)	3,622,716	Line_L5_PSDM_UnEnh.segy
L5: PSDM UnEnhanced (depth in meters)	2,147,676	Line_L5_PSDM_UnEnh_Meters.segy
L5: PSDM Interval Velocities	737,316	Line_L5_PSDM_Interval_Velocity.segy
L5: Unmigrated Time	3,886,116	Line_L5_Unmigrated_Time_Stack.segy
L5: PSTM Enhanced	3,958,112	Line_L5_PSTM_Enh.segy
L5: PSTM UnEnhanced	3,958,112	Line_L5_PSTM_UnEnh.segy
L11: PSDM Enhanced (feet)	27,409,764	Line_L11_PSDM_Enh.segy
L11: PSDM Enhanced (meters)	27,409,764	Line_L11_PSDM_Enh_Meters.segy
L11: PSDM UnEnhanced (feet)	27,409,764	Line_L11_PSDM_UnEnh.segy
L11: PSDM Interval Velocities	1,407,028	Line_L11_PSDM_Interval_Velocity.segy
L11: Unmigrated Time	6,138,048	Line_L11_Unmigrated_Time_Stack.segy
L11: PSTM Enhanced	6,138,048	Line_L11_PSTM_Enh.segy
L11: PSTM UnEnhanced	6,138,048	Line_L11_PSTM_UnEnh.segy
3D: Anisotopic PSDM Enhanced	153,678,840	Forge3d_ANI_PSDM_Stack_Enh.segy
3D: Anisotopic PSDM UnEnhanced	153,678,840	Forge3d_ANI_PSDM_Stack_UnEnh.segy
3D: Anisotopic PSDM Interval Vels	7,947,900	Forge3d_ANI_PSDM_INT_Velocity.segy
3D: Unmigrated Time	235,171,944	Forge3d_Unmigrated_Time_Stack.segy
3D: Poststack Time Migration Enhanced	235,171,944	Forge3d_Poststack_Time_Migration_ FXYDecon_Stack.segy
3D: PSTM UnEnhanced	121,067,944	Forge3d_PSTM_Stack_Enh.segy
3D: PSTM UnEnhanced	121,067,944	Forge3d_PSTM_Stack_UnEnh.segy
ALL: Digital Report	30,678,796	Final_Processing_Report_Forge.pdf

Table A1. List of all the stacked, processed files received from LSNS including Unmigrated Time, Prestack Time Migration (PSTM), Prestack Depth Migration (PSDM), Velocities used for migration, exact file sizes and file names. 301: 2D Line 301, 302: 2D Line 302, L5: Legacy Line 5, L11: Legacy Line 11, 3D: 3D Survey.

Line: Data Type	Size in bytes	File Name
3D: PSTM Gathers	7,991,116,080	Forge3d_PSTM_Gathers.segy
3D: PSTM Gathers (NMO removed)	7,991,116,080	Forge3d_PSTM_GathersUnNMO.segy
3D: Migration Velocities	6,687,900	Forge3d_PSTM_RMS_MigVel.segy
L5: PSTM Gathers	98,866,400	Line_L5_PSTM_Gathers.segy
L5: PSTM Gathers (NMO removed)	98,866,400	Line_L5_PSTM_GathersUnNMO.segy
L5: Migration Velocities	1,032,616	Line_L5_PSTM_RMS_MigVel.segy
L11: PSTM Gathers	147,230,352	Line_L11_PSTM_Gathers.segy
L11: PSTM Gathers (NMO removed)	147,230,352	Line_L11_PSTM_GathersUnNMO.segy
L11: Migration Velocities	311,028	Line_L11_PSTM_RMS_MigVel.segy
301: PSTM Gathers	276,362,772	Lin_301_PSTM_Gathers.segy
301: PSTM Gathers (NMO removed)	276,362,772	Lin_301_PSTM_GathersUnNMO.segy
301: Migration Velocities	723,924	Line_301_PSTM_RMS_MigVel.segy
302: PSTM Gathers	174,545,380	Line_302_PSTM_Gathers.segy
302: PSTM Gathers (NMO removed)	174,545,380	Line_302_PSTM_GathersUnNMO.segy
302: Migration Velocities	692,508	Line_302_PSTM_RMS_MigVel.segy

Table A2. List of all the unstacked, CMP gathers files received from LSNS including prestack time migration (PSTM) with and without Normal Moveout applied, velocities used for migration, exact file sizes, and file names. 301: 2D Line 301, 302: 2D Line 302, L5: Legacy Line 5, L11: Legacy Line 11, 3D: 3D Survey, RMS: Root Mean Squared

```
C 1 CLIENT: USGS/University of Utah PROCESSOR: Land Seismic Noise Specialists
C 2 LINE Forge3d AniPSDM Stack Enhanced     AREA Utah
C 3 YEAR ACQUIRED: 2017    YEAR PROCESSED: 2019
C 4 SAMPLE INT: 5m       TRACE LENGTH: 5000 m
C 5
C 6 COORD SYSTEM:METRIC GEODETIC DATUM:NAD83 UTM 12 N
C 7 PROJECTION:MOLODENSKY/TM
C 8
C 9 DATE:4/12/2019
C10 DATUM: 1800 m      REPLACEMENT VELOCITY: 2500 m/s
C12 CMP Bin : 25m x 25m
C13 PRODUCT: PSDM Stack Enhanced
C14 IL 1,   XL 1,  (332800.5,  4260778.0 )
C15 IL 170, XL 1,  (322874.25, 4265002.25)
C16 IL 170, XL 213,(338173.44, 4264910.0 )
C17
C18
C19
C20
C21 PROCESSING FLOW:
C22 GEOMETRY ASSIGNMENT AND QC,TRACE EDITS,REFRACTION STATICS.
C23 AIRBLAST DENOISE,SPECTRAL EDIT DENOISE,LSNS DENOISE
C24 QCOMP 100, DECON (OP 180 ms PRW 0.01%)
C25 VELOCITY ANALYSIS AND RESIDUAL STATICS LOOPS (TWO ROUNDS)
C26 VELOCITY ANALYSIS AND RESIDUAL STATICS LOOPS (TWO ROUNDS)
C27 POST DECON NOISE ATTENUATION -  SPECTRAL EDIT and DESPIKE
C28 RESIDUAL STATICS, AGC, Interpolation on OFFBINs, Anisotrpoic PSDM,
C29 BILATERAL FILTER OFFBINS, Bandpass 4-8-80-120 Hz, STACK
C30 FXY Decon 3x4 filter width
C31
C32 CMP_X: byte 189 4 byte ibm real
C33 CMP_Y: byte 193 4 byte ibm real
C34 BIN_ELEV byte 53 4 byte
C35 HEADER FOR FINAL DATUM CMP_STAT: byte 201 4 byte ibm real
C36
C37
C38
C39 SEG Y REV1
C40 END EBCDIC
```

Figure A1: Example of the EBCDIC text header from 3D processed file "Forge3d_ANI_PSDM_Stack Enh.segy". This file contains prestack depth migrated data. Year recorded, year processed, navigation coordinate system, survey endpoint coordinates, and processing flow are given. In addition, trace header locations for CMP X, CMP Y, CMP bin elevation and final datum static are provided which is sufficient to load the data into a seismic data interpretation system.

References

1. Barry, K.M., Cavers, D.A. and Kneale, C.W., 1975, Report on recommended standards for digital tape formats: Geophysics, 40, no. 2, p. 344–352, accessed January 26, 2016, at http://www.seg.org/resources/publications/misc/technical-standards.